UNIVERSITY OF TWENTE.

Faculty of Electrical Engineering, Mathematics & Computer Science

Development and characterization of an HNA etching process for realization of big sensor tubes

Xing An
M.Sc. Thesis
Nov.2020

Supervisors:
ir. Q.Yu
dr.ir. R.J.Wiegerink

Integrated Devices and Systems Group
Faculty of Electrical Engineering,
Mathematics & Computer Science
University of Twente
P.O. Box 217
7500 AE Enschede
The Netherlands

Acknowledgement

I would like to express great appreciation to my research supervisor Qihui Yu of the IDS group at the University of Twente, for his valuable and constructive suggestions during the development of my research work. He spent the time on the experiments for me when the cleanroom is unavailable to master students during the lockdown due to the pandemic. I would also like to express my deep gratitude to Dr. Remco Wiegerink for his patient guidance and enthusiastic encouragement of this research and passing on knowledge during my college career.

I would also like to extend my thanks to Meint de Boer, Sip Jan Boorsma, Remco Sanders for their exquisite technology and technical support.

Finally, I must express my very profound gratitude to my parents and to my friends for providing me with unfailing support and continuous encouragement throughout my years of study and through the process of writing this thesis.

Contents

Abstract

The microfluidic channel is the significant structure in a microflow sensor, which ensures to measure the laminar flow. A larger round channel can increase the flow rate and the measurement range and has benefits for increasing the accuracy and sensitivity of the micro Coriolis massflow sensor. The isotropic etching can etch a round channel based on the buried channel technology. The isotropic gas etchant such as XeF_2 can do that, but it will cost more after etching to a large diameter. HNA systems(hydrofluoric, nitric, acetic acid solution), as a wet isotropic etchant, can etch a large round channel in a low-cost way. In this thesis, an etching bath with an agitation system is designed and developed to meet the needs of HNA systems for rotation. After that, the round buried channel under a trench with $10\,\mu$m width and $65\,\mu$m depth is formed by HNA solution with a diameter of $100\,\mu$m and a smooth channel wall.

Chapter 1

Introduction

Microfluidic Lab on a Chip(LOC) and integrated microfluidic systems have gained enormous interest and noticeable capability over the past few years for many applicants in different fields involving (bio)chemistry, medicine, automotive, and industrial devices. Some of their properties are remarkable such as low fluid consumption, fast analysis and response times, accurate, reliable, and biocompatibility. Therefore, the flow sensors in these systems are of great concern as the pivotal components.

1.1 Motivation

The microfluidic channel is the significant structure in a micro flow sensor, which ensures to measure the laminar flow. A channel with a non-circular cross-section would be a factor that affects the accuracy because of its non-uniformity deformation with the pressure. Moreover, for increasing the flow rate, the larger diameter channels are made and can be used widely. Therefore, the channel with the circular cross-section and larger diameter is competitive in the microflow systems. For a Coriolis massflow sensor, the larger channel means that the ratio of flow mass and channel weight is high so that the magnitude of Coriolis force can be easy to detect and increase the sensitivity.

1.2 Micro thermal flow sensors

Most of the microflow sensors have been developed from the thermal measurement principle [1, 2]. These sensors can measure the flow down to the order of few nanoliters per minute and can be divided into three forms of thermal flow sensing: anemometric(hot-wire and hot-film), calorimetric, and time-of-flight.

A schematic figure of thermal sensors is shown in Figure 1.1 with the temperature distributions, which is simulated and plotted by COMSOL Multiphysics®. Three blocks indicated the electrodes in each sub-figure. The center one is the heater, and the other two are symmetrically placed about the center and used for sensing the temperature. In the case of Figure 1.1a, there is no flow in this environment. Hence the sensing values are equal. Once a fluid flow towards

to the right(in the case of Figure 1.1b), the temperature sensors on both sides will sense the different temperatures that are proportional to flow, as shown in Figure 1.2(e.g., the temperature sensors are placed on -40 and 40 of the x-axis).

(a)   (b)
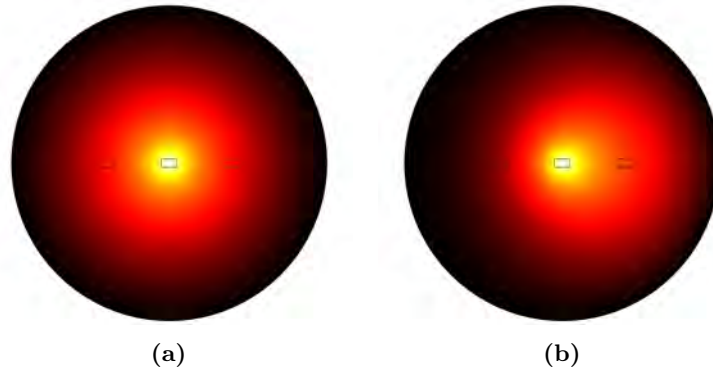
Figure 1.1: Schematic of thermal flow sensors with simulated thermal profiles, where the center block indicates heater and the symmetrical rests are the sensors in each figure. a) Temperature distribution without flow. b) Temperature distribution with a flow towards the right.
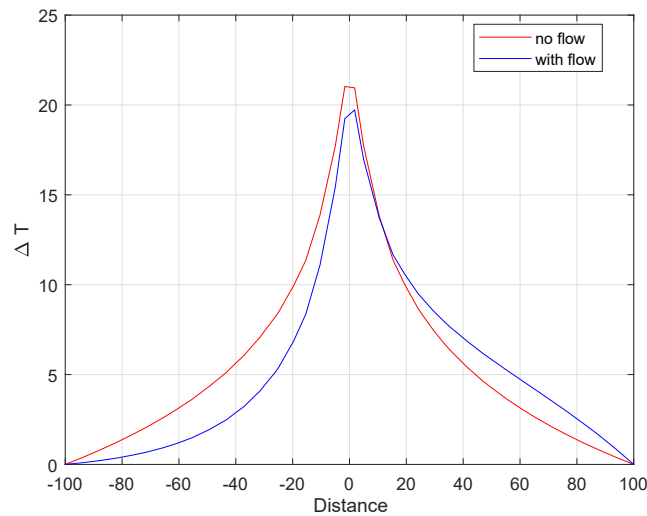
Figure 1.2: Schematic plot of temperature distribution against the distance along the longest horizontal cut-line, where the red line corresponds to Figure 1.1a and the blue one corresponds to Figure 1.1b. The heating element is located at 0 of x-axis, and other thermal sensors can be located on both sides of the heating element symmetrically, e.g. -40 and 40 at x-axis.

The sensing element of the anemometric flow sensor is a resistor that acts as a heater and a temperature sensor simultaneously and is depicted as the center block in Figure 1.1. When fluid with a lower temperature through the sens-

ing element goes up, the loss through convective heat increases from the joule heating that is generated by the resistor. The faster flow will result in more heat loss. Therefore the heat loss can be determined and calibrated for sensing applications to measure the flowrate.

The calorimetric flow sensor involves at least one temperature sensor that detects the thermal profile near upstream or downstream of the heating element due to the heat transferred by fluid flow. The flow results in asymmetrical temperature distribution upstream and downstream. The blue curve indicates the asymmetric of temperature distribution on both sides of the heater in Figure 1.2. The more flow implies, the more asymmetry degree, so the temperature difference is the key component to measure the flow rate.

Thermal time-of-flight flow sensors involve at least one heating element and one downstream temperature sensor. The heating component generates a short thermal pulse detected by the downstream temperature transferring to the surrounding fluid flow. The heating pulse's transit time from the heater to a thermal sensor is tracked, and extract flow rate information.

However, the accuracy of thermal flow sensors is affected by thin film materials applied and the impact of variable ambient temperature along with the distance. Besides the influence of the equipment itself and the environment, the fluid characteristics such as density and specific heat will also affect the measurement results [3]. Consequently, the fluid must be identified in advance, and the sensor needs to be calibrated for this fluid.

1.3   Micro Coriolis mass flow sensors

A Coriolis-type micro mass flow sensor consists of a vibrating channel, as shown in Figure 1.3. Coriolis forces can be detected when there is flow through the channel that is driven in actuation mode. Once a mass flow Φ_{m} goes through the tube, the Coriolis force F_{c} will appear, which can be expressed by

$$\vec{F}_{\mathrm{c}} = -2L_{\mathrm{x}}(\vec{\omega}_{\mathrm{act}} \times \vec{\Phi}_{\mathrm{m}}) \tag{1.1}$$

The Coriolis force leads to a secondary motion that can be detected (orthogonal to the actuation mode). Unlike other types of sensors, the Coriolis mass flow sensor measurement principle is independent of fluid properties. Without recalibration or conversion, the flow rate can be measured whether the fluid is liquid or gas. Since Coriolis mass flow sensors are operated at a particular resonance frequency, they can measure the density of fluid that is inverse proportional to the resonance frequency.
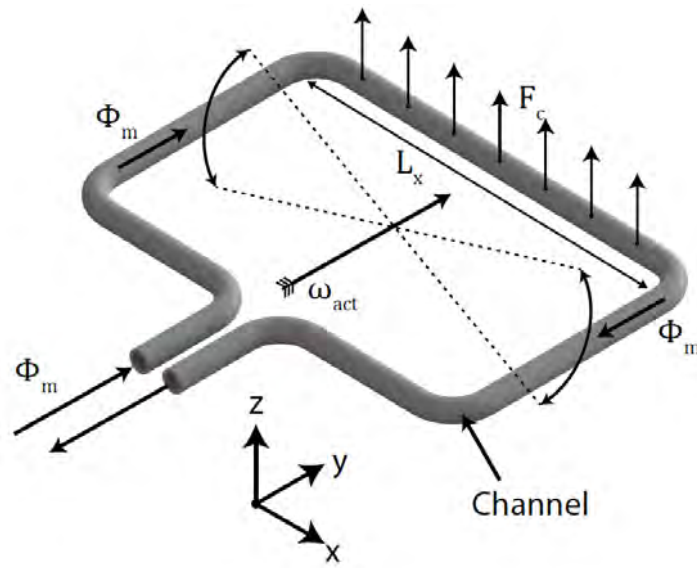
Figure 1.3: Schematic drawing of a rectangle-shaped Coriolis mass flow sensor. Where ω_{am} is the actuation-mode angular velocity, Φ_m is a mass flow flowing through the channel, L_x is the length of channel along x-direction, and F_c is the Coriolis force causing a secondary motion related to the mass flow [4].

Enoksson introduced the first micromachined Coriolis mass flow sensor in 1997 [5, 6]. It consists of two rectangular-shaped tube windows and measuring loops. Two etched wafers form the channel of the sensor by fusion-bonded technology. Each half-channel is etched in approximately $400\mu m$ deep in a silicon wafer using KOH anisotropic etching under a silicon dioxide mask. By using corner-mask compensations, all the convex corners were saved during the etching. The vibrating parts were etched by another KOH-etching step that leaves approximately $100\mu m$-thickness channel wall. The SEM image of the cross-section of the channel is shown in Figure 1.4.
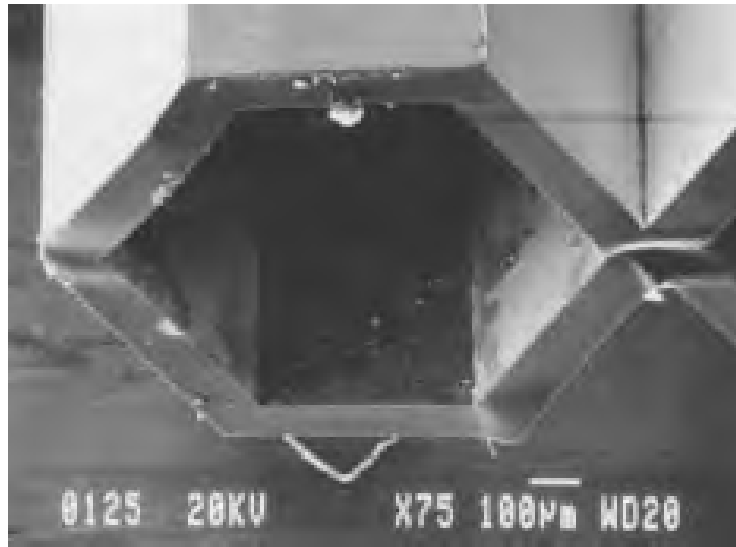
Figure 1.4: SEM image of the cross-section of the channels by Enoksson [6].

Another micromachined Coriolis mass flow sensor featuring a U-shaped measurement loop in a vacuum package was published by Zhang et al. [7], Sparks et al. [8] and Smith et al. [9] since 2001. The sensor was wafer bonded with two silicon half-channels that were etched by plasma. The Pyrex substrate was prepared by etching a cavity used to bond with the resonating channels and metal electrodes embedded. The fluid holes were drilled from the bottom to the inlets of the microchannels. The vibrating part of the sensor was actuated using electrostatic forces by the electrodes on the Pyrex substrate. Capacitive read-out was integrated by using metal electrodes.
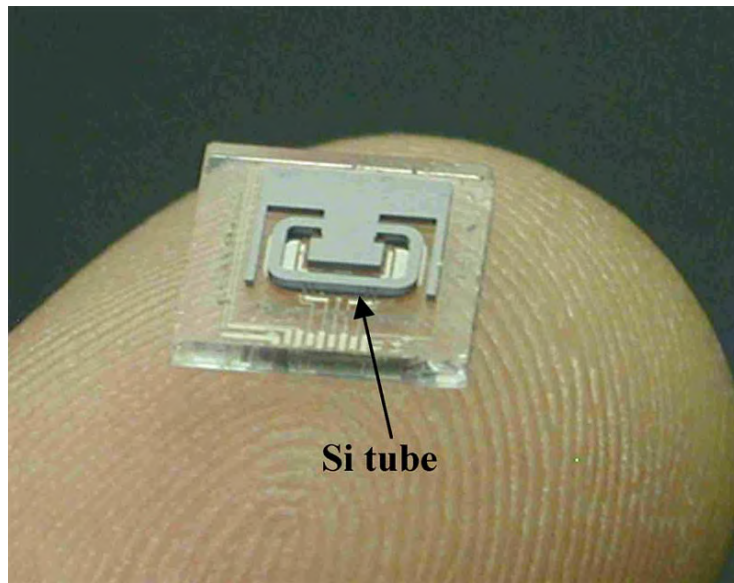
Figure 1.5: Micro Coriolis mass flow sensor by Smith et al. [9].
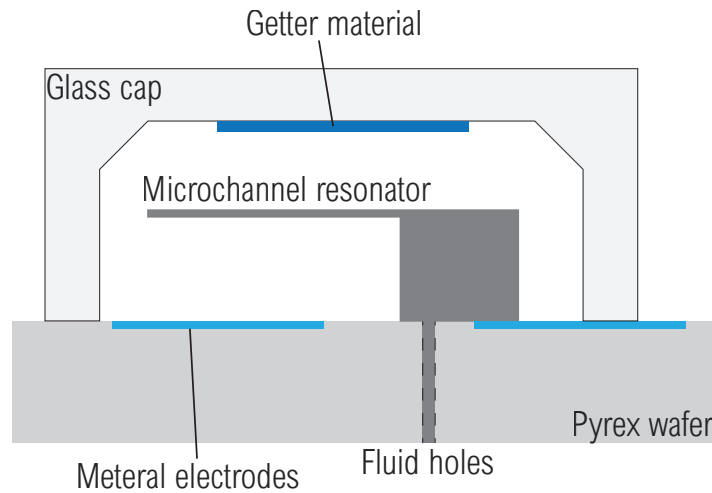
Figure 1.6: Side-view schematic of the resonating tube over the metal electrodes in vacuum package used by Smith et al. [9].

Haneveld et al. [10–12] presented a micromachined Coriolis mass flow sensor with a free-suspended rectangular measurement loop. The sensor has 40 μm diameter channels, which was developed by surface channel technology from Dijkstra et al. [13]. This sensor's vibrating part was fabricated by plasma etching semi-circular channels with a diameter of $40\mu m$ through small slits in a silicon nitride mask. The channel walls were formed by a $1.4\mu m$ thick silicon nitride layer. The metal layer was sputtered and patterned using lift-off lithography to form a metal track on the top of the channels for vibrating the tube by Lorentz

force. The silicon around the microchannel was etched by KOH etching from the backside of the wafer to make the channel free suspended. As for the front side, the fluidic access holes are etched by an RIE process. The view from the bottom of the channel is shown in Figure 1.7 and the complete sensor chip is shown in Figure 1.8.
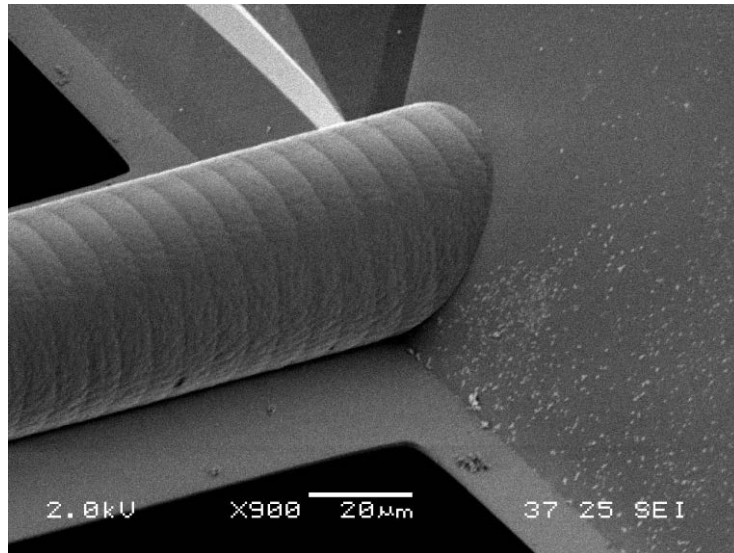
Figure 1.7: SEM image of the backside of the silicon-nitride channels [12].
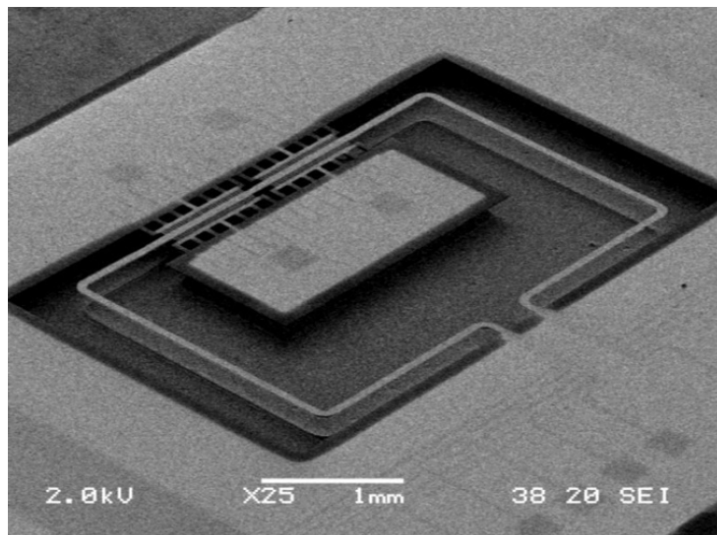
Figure 1.8: SEM image of the complete sensor chip [12].

In 2016, Monge et al. [14] presented a micro Coriolis mass flow sensor entirely fabricated in SU-8, as shown in Figure 1.9. Comparing with silicon-based

7

Coriolis mass flow sensor [10–12], staked layers of SU-8 significantly reduced the cost of fabrication, vacuum packaging. Although SU-8 was certainly not a suitable material for a resonant device since its intrinsic material losses result in the high damping effect during vibration, it is an option to find a compromise between costs and accuracy. The channel consists of $100\mu m$ thick channel walls and a squire internal cross-section with an edge length of $100\mu m$. Sensors use a metal layer on top of the sensor so that the channel can be actuated by Lorentz force.
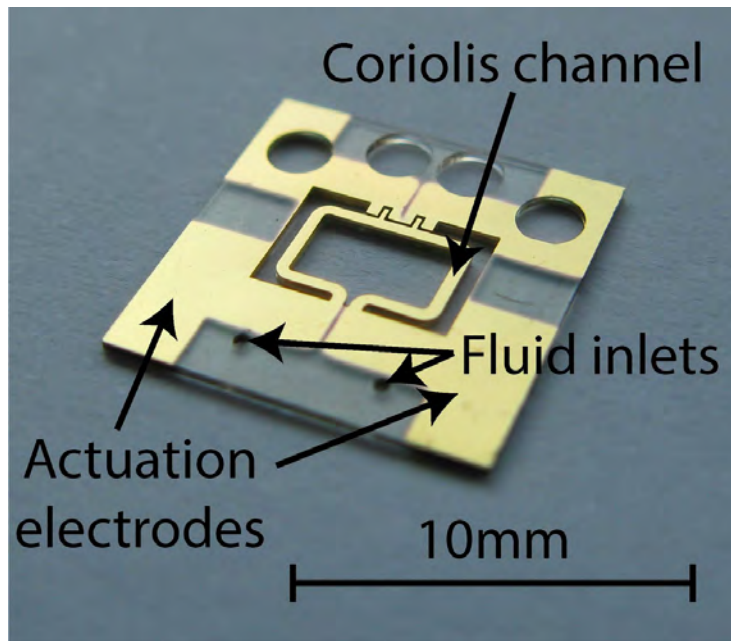

Figure 1.9: Photograph of the SU-8 Coriolis mass flow sensor presented by Monge [14].

1.4   Surface channel technology

With the need for size reduction of MEMS fluidic applications and devices in many fields, microchannels' fabrication to integrate various types of solid-state microfluidic structures is developed. These microfluidic structures usually have to be close to the fluid and bear the impact of fluid in physical or chemical. Furthermore, the microfluidic channels are often developed suspended freely to isolate the thermal from a substrate's heat-conducting and vibrate, move, or twist. For these purposes, the surface channel technology was developed to create quasi-semi-circular channels enclose in the silicon substrate.

Surface channel technology(SCT) is a technology that makes microchannels directly below the surface of the substrate, which is based on the buried channel technology(BCT) published by de Boer et al. [15] in 2000. The channels fabricated by SCT is completely sealed after processing, freely-suspended, low-stress, and some remarkable properties such as chemical-inert interfacing and integra-

tion of transducers. Therefore, some microchannels of thermal and Coriolis type microflow sensors and pressure sensors [10, 12, 16–18] were fabricated by/based on this semi-circular surface channel technology. The fabrication of the surface microchannels can be roughly described in three parts. First, a slit-pattern is applied to define the routine of the channel. The cross-sectional size and shape of channels can be modified by every single slit for different applications or purposes. Then the channels are etched by using a semi-isotropic etching method via the slits. Finally, a silicon-rich-nitride(SiRN) layer is deposited on the inner surface of the channel conformally to close the slits and to form a sealed channel [19].

(a)   **(b)**
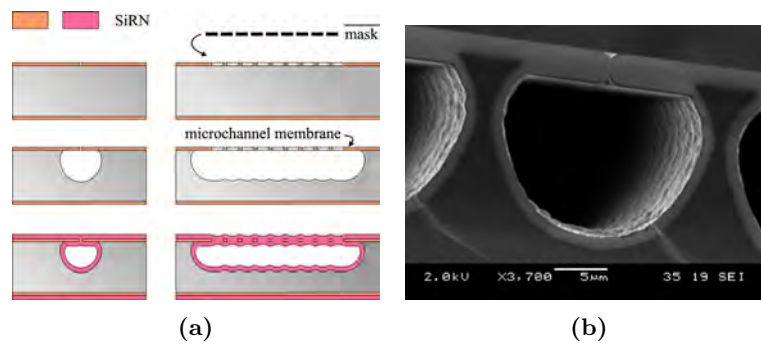
Figure 1.10: (a) Schematic of surface microchannel process. (b) SEM image of cross-section of sealed surface microchannels [13].

1.5   Buried channel technology

Due to the fabrication method's limitations, the channel's cross-section is never perfectly circular, as shown in Figure 1.10b. Consequently, the flat segment of channels will deform with pressure, and the flow rate is measured in a non-ideal way [17, 18]. A circular channel can reduce the effect of pressure compared with the channel with a flat segment.

To construct closed microchannels, besides the surface channel technology, some techniques can be used, such as anodic bonding and direct bonding at the wafer-to-wafer level and surface micromachining. The disadvantage of the former is that wafer-to-wafer misalignment and the microvoids may change or destroy the device's functional performance. The limitation of the latter technique is that the dimension is restricted by the sacrificial layer thickness, which can be deposited within a reasonable time period [15]. As an alternative method to conventional bulk and surface micromachining, Buried channel technology can form a sealed microchannel at different depths in bulk silicon. The fabrication process starts with a DRIE step that can etch a narrow trench in a certain depth. After SiRN protects the trench wall with applying low pressure chemical vapor deposition(LPCVD), an additional silicon oxide layer by plasma enhanced chemical vapor deposition(PECVD) is deposited for protecting SiRN on the substrate surface. The SiRN layer at the bottom of the trench is not covered by SiO_2 due to the high aspect ratio trench and low conformity and

bottom step coverage of PECVD. Then the SiRN coating at the bottom can be removed by plasma etching to allow the formation of the circular channel by either following isotropic wet or dry etching step.

Due to the less effect of pressure in the circular channel, the isotropically etching processes are needed for micromachining. For dry isotropic etching, some interhalogens gas etchants are normally used for silicon etching. The pure gaseous bromine trifluoride(BrF_3) has a high etching rate with a decent selectivity over silicon dioxide(SiO_2) [20] and makes smooth surfaces [21]. Xenon difluoride(XeF_2) has some advantages such as high selectivity for silicon and easy operation [22–26]. Normally XeF_2 is a white solid at room temperature and atmosphere pressure, and it can be sublimated into gas when the pressure is around 4 Torr [27]. XeF_2 is well known as isotropic etching, but vertical-to-lateral etch rate ratio(V/L ratio) is not equal to 1 all the time. At chip-level, the V/L ratio of XeF_2 is about 0.7 with larger than 4.5 Torr charge pressure [26] and the V/L ratio will be between 1.3 and 2 when the charge pressure is lower than 4 Torr [23, 24]. At wafer level, the V/L ratio of XeF_2 is between 0.9 and 1.1 within 40 to 100 etching cycles [27]. Chlorine trifluoride(ClF_3) is very similar chemical properties to BrF_3 and XeF_2. Compared with the low pressure environment of BrF_3 and XeF_2, ClF_3 has a suitable vapor pressure to achieve at room temperature [28].

Groenesteijn et al. [29] presented a fabrication process to fabricate large, free-suspended microchannels. The process is based on SCT and BCT to overcome their limitations. The difference is that the protective layer's material for the trench is silicon dioxide deposited by a thermal oxidation step. The selectivity of silicon to silicon dioxide is 1000:1 when XeF_2 is applied as an etchant. After thermal SiO_2 at the bottom, trenches are removed by directional plasma etching, and the channels can be etched by gas-phase XeF_2 isotropic etch through the trenches. It can be seen in Figure 1.11 that the cross-section of the channel is hexagonal with a diameter of around $80\mu m$.
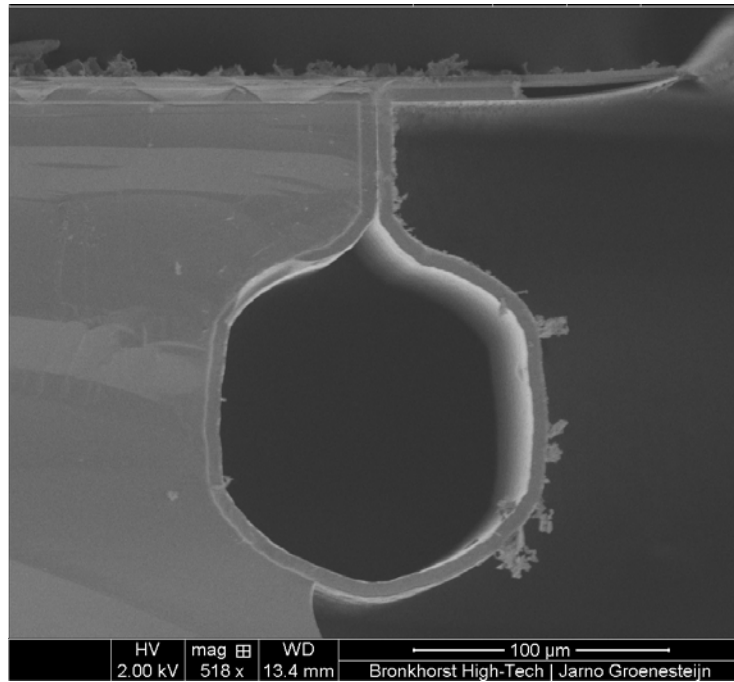
Figure 1.11: SEM image of cross-section of a partially released channel etched by XeF_2 and enclosed by SiRN [29].

For wet isotropic etching, HNA, a mixture of hydrofluoric acid(HF), nitric acid(HNO_3), and acetic acid(CH_3COOH), is a solution that can etch in all crystallographic directions at the same rate and make a rounded isotropic feature in single crystalline silicon. The silicon etch rates in HNA are independent of dopants and doping concentration but very sensitive to temperature and agitation [30]. The heat generated during the processing should be controlled. Otherwise, the runaway reaction happens and causes non-uniform etching and rough etching surface on silicon [31]. The moderate agitation can help the high uniformity and low roughness of etching [31–33]. H_2O is also the diluent that can replace acetic acid in the HF-HNO_3 system, but CH_3COOH shows a much better tolerance than water as the diluent because it can prevent the excessive dissociation of HNO_3 better and enhance the oxidizing power of HNO_3 [32,34,35], but excessive addition of CH_3COOH can cause an erratic etch rate [30] and reduce the oxidizing power of HNO_3 [34].

1.6   Aim of research

As mentioned above, the cross-section of microchannel fabricated by SCT is semi-circular. Once the pressure goes up, the channel will not deform uniformly on the cross-section perpendicular to flow direction. To sum up, the buried channel technology is introduced to this assignment to achieve micromachining a channel buried underneath the wafer's surface. Based on the buried channel technology, the etching will start at a certain depth. After the trench's

bottom opened, the wet isotropic etch will be applied for etching a circular channel with HNA systems. Due to the long etching time, the uniformity and the reproducibility are challenging to ensure. In order to improve these, a new experimental setup with an agitation system is introduced into the wet etching process.

1.7   Thesis outline

Chapter 2 introduces the HNA theory and its published applications. Chapter 3 describes the design details of the etching bath and the operation manual. Chapter 4 shows the preparation for wafers to be etched by HNA, including the fabrication process, experiment setup, and observation method afterward. In Chapter 5, the results are discussed.

Chapter 2

Channel fabrication using wet isotropic etching by HNA systems

A mixture of hydrofluoric acid, nitric acid, and acetic acid(HNA) is used as an isotropic wet etchant for etching silicon and polysilicon. This chapter is split into two parts: one part deals with the theory of HNA systems and the other with paper review related to etching microstructures with detailed quantitative parameters in HNA systems. The reaction mechanisms, runaway reaction, mask selection, and the influence factors of the HNA system during etching are introduced in the theory part. In the second part, some microstructures etched by HNA systems from other research groups are reviewed. In these reviewed papers, during the etching process by HNA, some factors affecting the results are concerned, such as HNA compositions, the physical auxiliary devices, and temperature control. Finally, a comparison of critical factors among those papers is listed and is a reference for the following experiments.

2.1 Introduction

HNA solution is an etchant that is widely used in wet isotropic etching. One of our goals is to etch a channel with a diameter up to $300\mu m$ through a trench with a $10\mu m$ width and a certain depth underneath the wafer. As introduced in the last chapter, an $80\mu m$ diameter buried channel was etched successfully by XeF_2. Although the channel can be etched to a higher diameter by applying more cycles of etchant, the cost increases more, and the etch rate on radius reduces. In other words, the etching efficiency goes down continuously.

Another point is that the cross-section is hexagonal, as shown in Figure 1.11. The vertical-to-lateral etch rate ratio is not equal to 1 all the time and can be varied in order of 0.1 Torr changes. Comparing with XeF_2, for the buried channel, HNA has more advantages such as less cost, more isotropic, working at atmosphere. Therefore, HNA is selected as the wet isotropic etchant in the

etching process.

2.2 Theory of HNA systems

Wet etching is a material technology and widely used in the field of silicon bulk micromachining. Isotropic wet etching is one of the wet etching methods that can etch silicon in any direction in the same etch rate. When etching silicon with aggressive acidic etchants, rounded isotropic patterns form. The method is widely used for [35]:
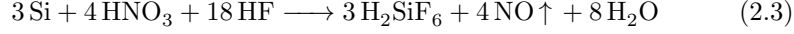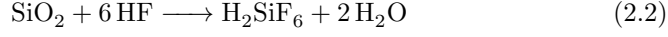
1. Removal of work-damaged surface layer caused by physical processes such as mechanical machining or ion bombardment,

2. Rounding of sharp anisotropically etched corners(to avoid stress concentration),

3. Removing of roughness after dry or anisotropic etching,

4. Creating structures or planar surfaces in single-crystal slices(thinning),

5. Patterning single-crystal, polycrystalline, or amorphous films,

6. Delineation of electrical junctions and defect evaluation(with preferential isotropic etchants).

7. Fabrication of sharp microneedle tips on a wafer [36],

8. Fabrication of concave hemispherical profiles on a wafer [36].

For isotropic etching of silicon, the most commonly used etchants are mixtures of nitric acid and hydrofluoric acids. In the case of HNO_3, water can be used as the diluent, but acetic acid(CH_3COOH) is preferred because it prevents the excessive dissociation of the nitric acid better and thus preserves the oxidizing power of HNO_3 [35].

2.2.1 Reaction mechanism

The most popular etchant for isotropic wet etching is the $HF-HNO_3$ system. HNO_3 is the oxidation agent, HF is the reducing agent(or complexant agent [30]) and CH_3COOH is neutralizing agent [37]. The HNA etching mechanism is reported in a series of papers by Robbins and Schwartz [34, 38–40]. Generally, silicon etching in HNA can be formally divided into two consecutively proceeding processes:

1. the formal oxidation of Si to SiO_2 by HNO_3, Reaction 2.1.

2. the formal dissolution of the SiO_2 by HF under release of a new silicon surface, Reaction 2.2.

$$3\,\text{Si} + 4\,\text{HNO}_3 \longrightarrow 3\,\text{SiO}_2 + 4\,\text{NO}\uparrow + 2\,\text{H}_2\text{O} \qquad (2.1)$$

$$\text{SiO}_2 + 6\,\text{HF} \longrightarrow \text{H}_2\text{SiF}_6 + 2\,\text{H}_2\text{O} \qquad (2.2)$$

$$3\,\text{Si} + 4\,\text{HNO}_3 + 18\,\text{HF} \longrightarrow 3\,\text{H}_2\text{SiF}_6 + 4\,\text{NO}\uparrow + 8\,\text{H}_2\text{O} \qquad (2.3)$$

The overall etching reaction is shown in Reaction 2.3. The Reaction 2.2 also have other intermediate products, Reaction 2.4.

$$\text{SiO}_2 + 4\,\text{HF} \longrightarrow \text{SiF}_4\uparrow + 2\,\text{H}_2\text{O} \qquad (2.4)$$
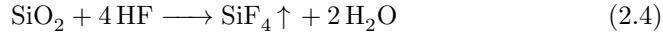
Nitric acid oxidizes silicon atoms taking electrons away from the surface and leaving holes behind. That way, silicon becomes susceptible to the nucleophile an attack of HF or $\text{F}^-$. In other words, that silicon becomes easy to reaction with HF or F^-. One by one $\text{Si}-\text{F}$ bonds are formed until SiF_4 detaches from the surface and diffuses to bulk solution [41]. If there is an excess of HNO_3, the oxidation of silicon proceeds much faster than the formation of $\text{Si}-\text{F}$ bonds. Therefore, the etching process becomes independent of the crystal orientation.

The HNA reaction mechanism could also be explained in another way. The silicon etching process involves hole injection into the silicon valence band by an oxidant, an electrical field, or photons. The holes attack the covalently bonded Si, oxidizing the material, followed by a reaction of the oxidized Si fragments with OH^- and subsequent dissolution of the silicon oxidation products in HF. The etching of the silicon by HNA solution can be written by the following reactions:

$$\text{HNO}_3 + \text{H}_2\text{O} + \text{HNO}_2 \longrightarrow 2\,\text{HNO}_2 + 2\,\text{OH}^- + 2\,\text{h}^+ \qquad (2.5)$$

The holes h^+ in Reaction 2.5 are generated in an autocatalytic process; HNO_2 generated in the above reaction re-enters into the further reaction with HNO_3 to produce more holes. With a reaction of this type, there is an induction period before the oxidation reaction takes off until a steady-state concentration of HNO_2 has been reached. This induction period has been observed at low HNO_3 concentration. After hole injection, OH^- groups attach to the oxidized Si species to form SiO_2, liberating hydrogen in the process [35]:

$$\text{Si}^{4+} + 4\,\text{OH}^- \longrightarrow \text{SiO}_2 + \text{H}_2\uparrow \qquad (2.6)$$
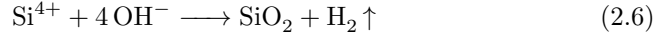
HF dissolves the SiO_2 by the forming the water-soluble H_2SiF_6. The overall reaction of HNA with Si:

$$\text{Si} + \text{HNO}_3 + 6\,\text{HF} \longrightarrow \text{H}_2\text{SiF}_6 + \text{HNO}_2 + \text{H}_2\text{O} + \text{H}_2\uparrow \qquad (2.7)$$
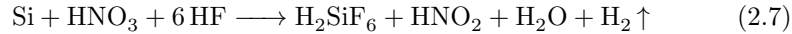
The simplification in the above electrochemical component of the reaction scheme is that only holes are taken into account. In the actual Si acidic corrosion reaction, both holes and electrons are involved. The reactivity of a hole injected in the valence band is significantly higher than that of an electron injected in the conduction band [35].

2.2.2   Runaway reaction

Hui et al. [31] reported that the way that prevents a runaway chemical reaction in the HNA solution. The runaway reaction happened when the heat generated and the HNO_2 has not been dissipated by enough solution for a large etching silicon area. When a runaway reaction occurs, bubbles and a lot of yellowish-brown nitrogen dioxide gas will be coming out, resulting in non-uniform etching and will destroy the specular surface formed by the etching earlier. HNA is an autocatalytic etchant, and the HNO_2 generated is usually required to keep the reaction going. In order to keep the HNO_2, at the beginning of etching, it is desirable to keep the mass transfer low. A small amount of heat conduces to accelerate the reaction. According to the Reaction 2.5, it needs one HNO_2 to start the reaction. This reaction will produce two HNO_2 as one of the end products, and HNO_2 becomes the starting reagent to catalyze the reaction. As a result, the longer the reaction takes place, the more the HNO_2 it will have. If the solution is standing alone without any stirring or agitation, HNO_2 will sink to the bottom of the container since it is heavier than water. In order to control the reaction rate, dissipating the HNO_2 and the heat generated is necessary during etching. Proper stirring is a benefit to help the reaction to proceed smoothly. One the other hand, too much stirring may eliminate the HNO_2 generated to fuel back the reaction and thus makes the reaction rate too slow. The volume of the HNA solution should be enough to prevent the runaway reaction. Less volume of HNA solution leads high concentration of HNO_2 and high temperature during etching. Hence it is essential to watch out for the etch-area:etchant-volume ratio.

Figure 2.1: Photograph of the runaway reaction by 12.5 ml of an HNA solution with HF:HNO_3:CH_3COOH = 2:4:4, on a 35 mm ×35 mm silicon piece. [31]. The dense brown NO_2 gas formed and the timer shows the time after reaction started.

When a runaway reaction occurs, as shown in Figure 2.1, the solution will be bubbling, and a lot of yellowish-brown nitrogen dioxide will be coming out. The reaction rate will be accelerated much faster and hard to control, because

of HNO_2 and increasing temperature. Runaway reaction can cause non-uniform etching, and it will give a non-optical surface formed.

2.2.3   Mask selection

HNA solution has not only powerful corrosion characteristics on silicon but also the ability to etching mask material. Although there is a decent selectivity between silicon and mask material, the diameter of a big buried tube is restricted by the mask material and mask thickness.

Silicon dioxide has an etch rate of $300\,\text{Å/min}$ to $800\,\text{Å/min}$ in the $HF:HNO_3$ system, thick layers of thermal SiO_2 often are used as mask because of ease of patterning in a limited etch time. Chemical vapor deposited SiO_2 at $450\,°C$ has $0.44\,\mu m/min$ that is not applicable for a long term wet etch. LPCVD SiRN is the preferred masking material with the etch rate of $10\,\text{Å/min}$ to $100\,\text{Å/min}$ in HNA.

2.2.4   Influence factors of HNA

Theoretically, the etch rate of isotropic wet etching is the same in all directions. However, having the same etch rate in every direction is not easy to achieve during the practice etching process, which is affected by experimental factors in reality.

Effect of stirring or rotation on isotropic wet etching

The etchant is limited by the diffusion during isotropic wet etching. The etch rate goes down as the etching progresses in a narrow space. As a result, the etch rate in each direction is not equal, and it will lead to anisotropic results. Chemical mass transport issues generally keep such etchants from exhibiting perfectly isotropic properties, and the function of agitation is to help speed the transport of reactants and products and to keep the transport more uniform [42].

The shape of the microstructure HNA etched is affected by agitation. The etchant moves downward and outward through an opening in the mask and enlarges the etched groove in a vertical direction. The resulting isotropically etched features show more symmetry and rounding when agitation accompanies the etching. This agitation effect is diagrammed in Figure 2.2. The etched features approach a more ideal round hemisphere with agitation, but without agitation, the profile resembles a rounded box [43]. Rotating agitation assists etchant and products to the silicon surface equality while bringing more reactants to the surface, accelerates the etching and makes solution concentration distributing uniformly.

Silicon etch rate is susceptible to the agitation [30]. Several studies showed that agitation affects the rate and uniformity of isotropic etching. Agitations could help maintain the concentration of etchant [32] and remove the bubbles away from the surface for further increasing the surface quality [44]. There are some gases intermediate products such as NO, H_2, SiF_4, and NO_2 probably during reaction. The inevitable generation of reaction products has a major

influence on the surface of silicon. The gas bubbles interrupt the etching process locally. It could be the reason why the channel has a non-optical surface quality and unacceptable uniformity.

ISOTROPIC WET ETCHING: NO AGITATION

ISOTROPIC WET ETCHING: AGITATION

Mask

Figure 2.2: Schematic of agitation effects on isotropic wet etching.

Effect of HNA compositions on isotropic wet etching

Schwartz and Robbins published four detailed papers between 1959 and 1976 [34, 38–40]. The effect of HNA compositions on isotropic wet etching was well characterized and described in these four papers. The results of HNA etching by weight percentage of various components are expressed in the form of isotropic etching curve, as shown in Figure 2.3. The concentration of HF and HNO_3 are 49 weight percentage(wt%) and 69 wt% respectively. Water as diluent is marked by dashed-line curves, and the acetic acid is indicated by solid-line curves.
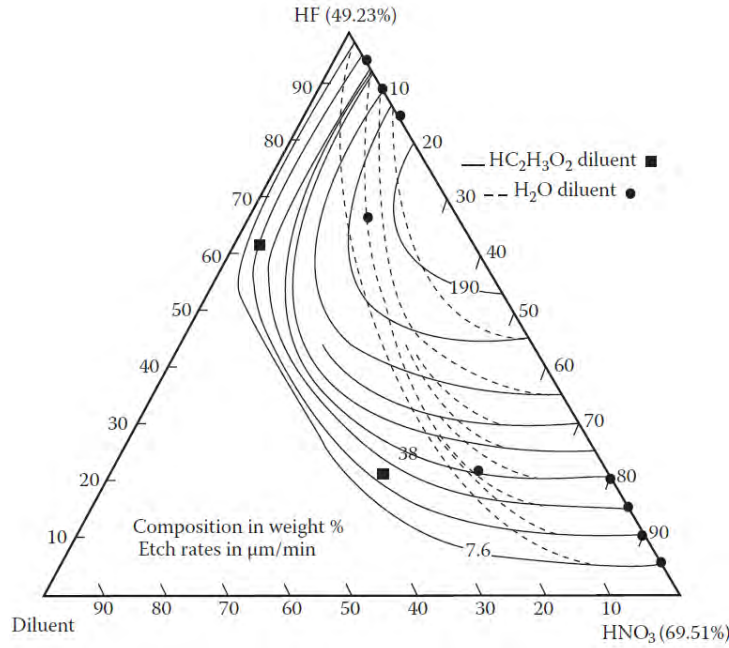
Figure 2.3: Isotropic etch curves, contours of change of die thickness as function of etchant composition in HNA system. Recalculated for one-sided silicon etching and expressed in μm min^{-1} [35] from H.Robbins and B.Schwartz [39].

It can be seen that the compositions of HNA have obvious effects from Figure 2.3. Some characteristics can be summarized from these curves [35]:

At the top part of the composition triangle, it stands for the high HF and low HNO_3 concentration. The solid curves are parallel to the HF axis, which represents the constant concentration of HNO_3 in every single solid line. Consequently, the HNO_3 concentration dominates the etch rate. A layer of SiO_2 grows slowly in this concentration, and the surface of silicon becomes unstable and rough. The etch is limited by the rate of oxidation. The activation energy in the high HF region is in the range of about 20 kcal/mol [40] for CH_3COOH diluent. Therefore the temperature influence is more pronounced.

At the right bottom of the composition triangle, the solid-curves are parallel to the diluent axis(solid line stands for the CH_3COOH diluent). It is at constant HF composition. Etches in this regime are isotropic and have a smooth surface. In this regime, the etch rate is controlled by the ability of HF to remove the SiO_2 formed from oxidation of HNO_3(Reactions. 2.2 and 2.4). It is typically limited by diffusion of HF reaction above room temperature. This diffusion-limited process has lower activation energy(4 kcal/mol [40]) than the case in the previous paragraph. Therefore, temperature changes are less significant.

Acetic acid is less polar than water and helps prevent the dissociation of HNO_3(undissociated HNO_3 is the primary oxidant) [35,39], thereby allowing the

formation of more of the species directly responsible for the oxidation of silicon. Moreover, the acetic acid gives the surface of etched silicon a smooth finish. In theory, the wetting action of acetic acid prevents the formation of bubbles during surface etching [45]. Furthermore, acetic acid also influences the etch rate of silicon nitride. The etching rate comparison of silicon nitride in etching solutions with and without acetic acid is shown in Figure 2.4. The top row in the x-axis label indicates the ratio of HNA compositions in $HF:HNO_3:CH_3COOH$ and the bottom row stands for $HF:HNO_3$. It is clear to see that the addition of CH_3COOH does not give much influence on the etch rate of silicon nitride as the low ratio of HF(at first four compositions). However, when the ratio of HF occupies over 40%, the etch rate with CH_3COOH is lower than the one without CH_3COOH. At the left bottom of the composition triangle, the HNA has a shallow etching rate [36].
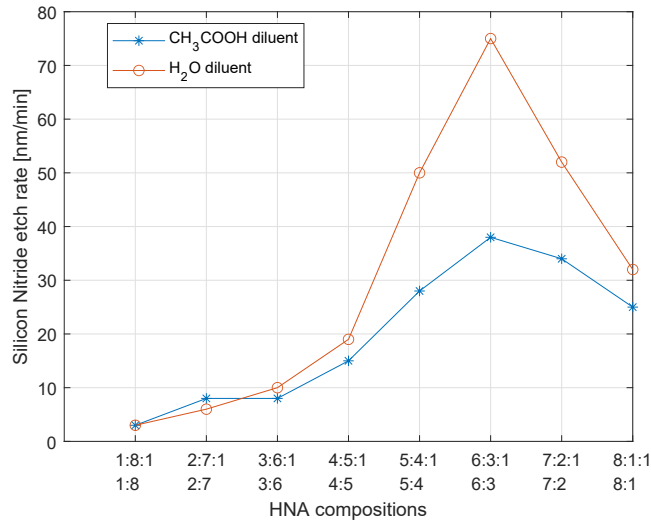
Figure 2.4: Etching rate comparison of LPCVD mask in etching solutions with and without acetic acid [46]. Ratios $HF:HNO_3:CH_3COOH$ and $HF:HNO_3$ are indicated on top row and bottom row respectively at x-axis.

Effect of temperature on isotropic wet etching

The temperature effect has to be discussed with compositions in HNA systems because the activation energy of the reaction is different in the different HNA composition regions. It would be better to be explained with some practical cases in Section 2.3.

2.3   Review

HNA is one of the most widely used isotropic wet etching solutions in silicon bulk machining [22], which is the etchant applying on many microstructures, such as acoustic lenses [47], semicircle cross channels [44, 48], microneedles [49, 50], and

hemispherical resonators [51].

Many factors of the HNA system affect the results during the etching process, as mentioned above. Each microstructure to be produced has particular etching parameters to achieve specific innovations such as high uniformity, circularity, repeatability, and low roughness. Some characterizations of the HNA system in published articles relating to different applications from other groups are reviewed, which can be referenced for the big tube etching. In this section, the HNA compositions, physical auxiliary method and etching temperature of each article are mainly discussed and evaluated by the uniformity, etch rate, mask selectivity, roughness and circularity.

### 2.3.1   Application 1: microneedles

Hamzah et al. [49] presented the fabrication of the high aspect ratio solid silicon microneedles that are suitable for transdermal drug delivery applications, as shown in Figure 2.5. The HNA etching parameters were characterized by varying the HNA composition, the optical mask's window size, etching temperature, and the etch bath agitation to optimize the long and narrow bodies with smooth surfaces wafer. To achieve optimal etching parameters for high aspect ratio of microneedles, an L9 orthogonal Taguchi experiment with three factors(agitation rate, mask window size, and HNA composition), each having three levels, was utilized. The parameter combination of an HNA composition of 2:7:1($HF:HNO_3:CH_3COOH$), a window size of $500\,\mu m$ and agitation rate of 450 RPM were deemed as the optimum solution for these silicon microneedles, which was suggested by Taguchi experiment.
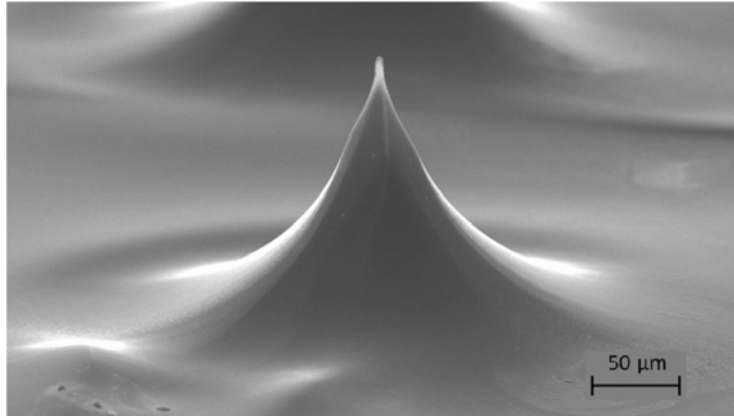
Figure 2.5: SEM image of microneedles that is etched by HNA with deemed optimal for producing the high aspect ratio solid silicon microneedles usable for transdermal drug delivery application [49].

The HNA of etching the microneedles on a wafer surface was characterized in HNA compositions, size between arrays, and temperatures. The purpose is to exploit etching parameters to control vertical etch rate against the lateral for forming a high aspect ratio needles while producing a sufficiently smooth

surface. For testing the effect of HNA compositions on the microneedles profile, nine compositions of HF and HNO_3 without CH_3COOH, and also eight compositions with 10% CH_3COOH were set, as listed in Table 2.1. The samples having arrays of $200\,\mu m$ diameter circles and $200\,\mu m$ spaced were immersed in $30\,ml$ HNA solution at $20\,°C$ without agitation and were placed face up at the bottom of Teflon beaker. An isoetch contours for HNA composition with 0% and 10% acetic acid concentrations are present in Figure 2.6, and the vertical and lateral etching measurements are listed in Table 2.1.
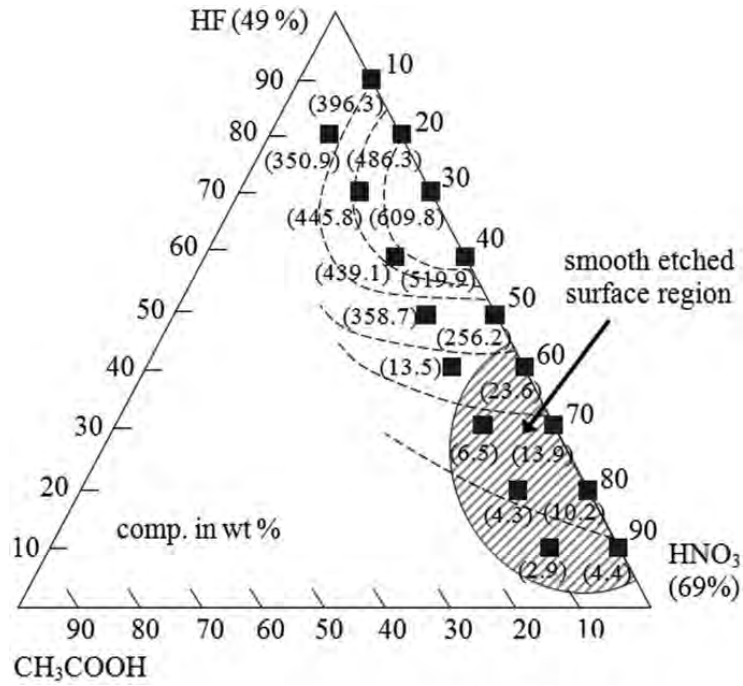
Figure 2.6: Isoetch contours of vertical etch rates(μm min^{-1}) on microneedles [49].

Table 2.1: Vertical an lateral etch rates of silicon for various HNA compositions are tested for microneedles arrays with $200\,\mu$m diameter and $100\,\mu$m space under Si_3N_4 mask layer [49].

HF:HNO$_3$:CH$_3$COOH (vol.ratio in percent)	Vertical etch rate (μm min^{-1})	Lateral etch rate (μm min^{-1})	% Difference
10:90:0	0.65	0.69	-5.79
20:80:0	1.00	1.01	-0.99
30:70:0	1.14	1.15	-0.86
40:60:0	1.28	1.36	-5.88
50;50:0	2.41	2.38	1.26
60:40:0	2.72	2.62	3.82
70:30:0	2.79	2.75	1.45
80:20:0	2.69	2.67	0.75
90:10:0	2.59	2.58	0.39
10:80:10	0.45	0.46	-2.17
20:70:10	0.64	0.65	-1.54
30:60:10	0.81	0.83	-2.41
40:50:10	1.13	1.14	-0.88
50:40:10	2.55	2.42	5.37
60:30:10	2.64	2.51	5.18
70:20:10	2.55	2.56	-0.39
80:10:10	2.50	2.48	0.81

In Table 2.1, the percentage differences between vertical and lateral etch rates are less than 6% in their case in last column. The difference is calculated by

$$\text{Difference} = (\frac{\text{Vertical}}{\text{Lateral}} - 1) \times 100\% \qquad (2.8)$$

The HF:HNO$_3$:CH$_3$COOH volume ratio of 2:7:1 was selected for the following characterization tests because it would produce a smooth surface while having an acceptable etch rate.

In testing for the effects of etching temperature, samples with $100\,\mu$m space were dipped in a 30 ml 2:7:1 HNA solution for 3 min in $10\,°$C, $30\,°$C, $35\,°$C, $40\,°$C and $50\,°$C. The vertical and lateral etch rates steadily increase up to $35\,°$C and both rates are similar, as shown in Figure 2.7. However, excessive oxidation was observed, with the solution rapidly turning golden yellow and producing thick vapor at temperature beyond $35\,°$C, indicating rapid uncontrollable etching, as mentioned the runaway reaction at Section 2.2.2.
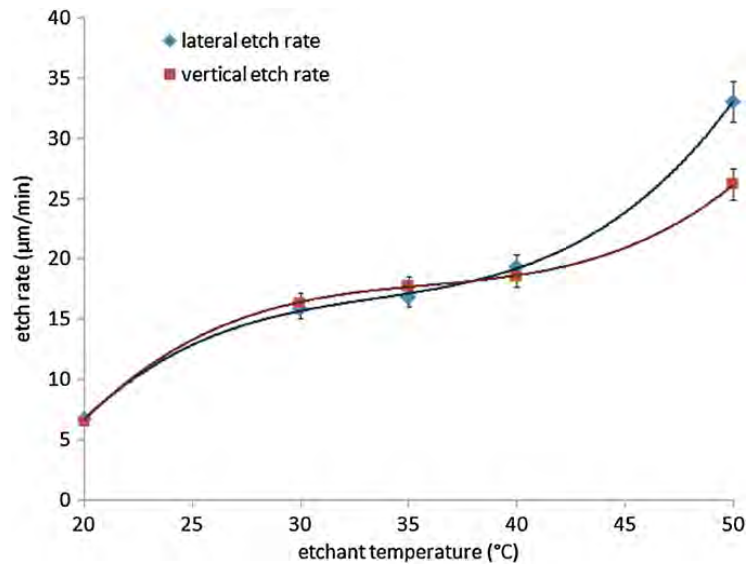
Figure 2.7:   Plot of etch rates versus temperature for the 2:7:1 (HF:HNO$_3$:CH$_3$COOH) solution [49].

The HNA characterization with an agitation system was tested by an HNA etch bath with a stirrer bar driven by an external magnetic power source. The orientation of the sample immersed in the HNA solution was towards to the tangential direction of flow for achieving the high vertical versus lateral etch rate differential, as shown in Figure 2.8. The magnetic stirrer bar was placed at the bottom of the Teflon beaker. The flow rate of the HNA solution was controlled by the magnetic stirrer and was proportional to the rotation speed. The rotation speeds were tested in 150, 250, 350, 375, 400, 425, and 450 RPM.
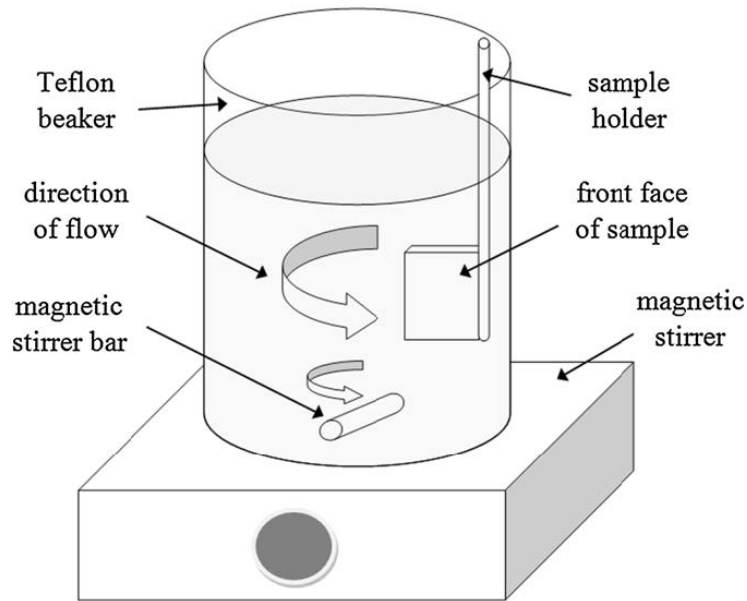
**Figure 2.8:** Hamzah stir setup for microneedles [49]

According to these HNA characterization tests, it is observed that HNA composition does not influence the V/L ratio without agitation from Table 2.1, but affects the roughness of the etched surface. Etching in high temperatures is unfavorable, especially as the temperature is higher than 35 °C, which causes uncontrollable, rapid, and anisotropic etching with the composition of 2:7:1. Due to the orientation of samples placed in the etch bath, the vertical and lateral etch rates were no longer similar to agitation. Therefore, the HNA compositions around 2:7:1 are learned and will be tried in the big tube experiments.

Bhandari et al. [50] presented that a wafer-scale etching method to increase the geometrical uniformity for their microelectrode arrays(Utah electrode array, UEA, shown in Figure 2.9) that is applying on recording and stimulating neural tissue. Before the wet etching process, the preparation was very straightforward to make a similar profile of microelectrode arrays. A 2 mm thick 75 mm diameter wafer was cut two orthogonal sets of deep kerfs directly by a Disco dicing saw. The etching process by HNA consists of two steps - dynamic etching and static etching. The former is that the sample wafers were etched in an agitation system. The wafer lays on the bottom for the other one.
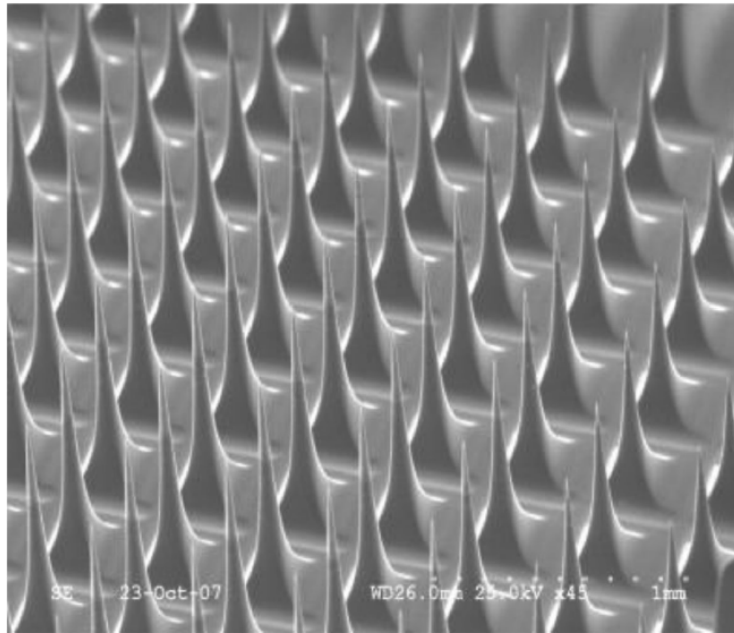
Figure 2.9: SEM image of Utah electrode arrays [50].

The temperature and agitation characterizations of HNA in their work were tested, which affect on the etch rate and the uniformity. For temperature characterization, the samples wafers were immersed in 1500 ml of etching solution(acid mixture of HF(49%)-HNO$_3$(69%) in ratio of 1:19) for each test and the temperature was varied from 20 °C to 60 °C. The wafer were etched for 4 min each time. The etch rate and non-uniformity against temperatures is shown in Figure 2.10. It is clearly to see that the non-uniformity is lowest at temperature of around 20 °C. The etch rate was not affected much by temperature changing.
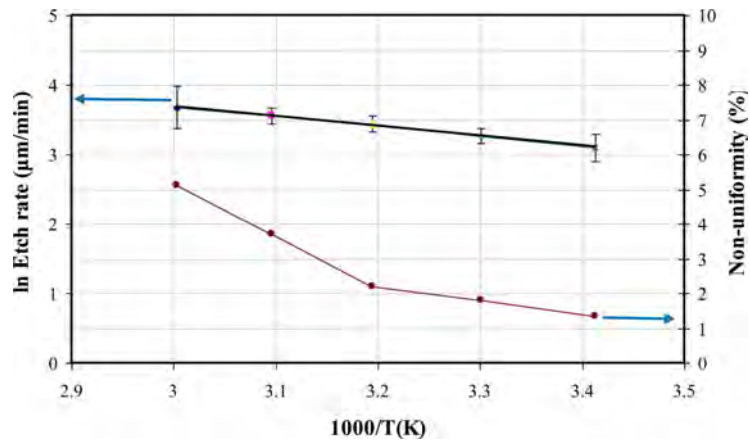
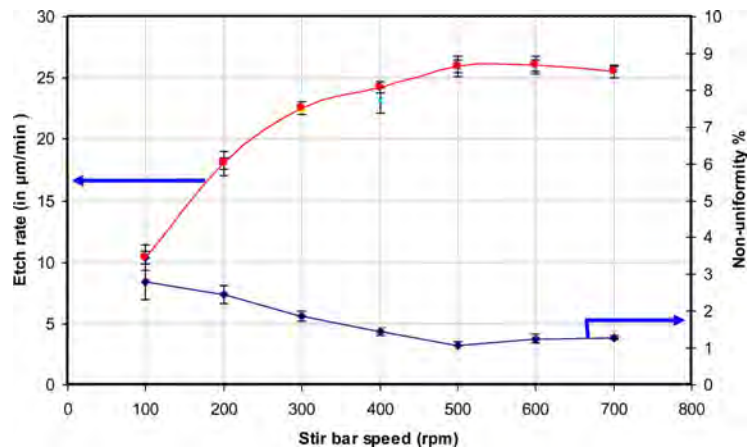**Figure 2.10:** Arhenius plot of etch rate and non-uniformity as function of temperature [50].

An experiment was carried out to determine the effect of agitation on the

rate and uniformity during dynamic etching. The agitation setup is shown in Figure 2.11. A 2.5 inch stirrer bar was driven by a magnetic power source with a rotation rate varying from 100 RPM to 700 RPM. The etching was carried out each time for 4 min.

Figure 2.11: Agitation setup for UEA. The wafer holder and stirrer bar can rotate in opposite direction [50].

The etch rate and non-uniformity as a function of stirrer bar rotation speed is shown in Figure 2.12. With increasing the stirring speed, the non-uniformity decreases clearly, and the etch rate increases a lot.

**Figure 2.12:** Plot of etch rate and non-uniformity against stir bar speed [50].

In summary of this application, both applications have some common points. Their microstructure has large microloading, which leads to the fast consumption of acidic in the HNA solution. The stirring speed would increase to at

least 500 RPM to achieve uniformity due to the large area of silicon exposed to the etchant. For getting a smooth surface, it is better to keep the solution temperature around room temperature.

### 2.3.2 Application 2: hemispherical toroidal silicon molds

Bai et al. [32] presented a wafer-scale etching method used to create the toroidal mold of hemispherical resonator gyroscope(HRG), which is based on the deep reactive ion etching and improved HNA isotropic etching. With this method, they fabricated good toroidal molds with $1900\,\mu m$ diameter, less than 0.2% asymmetry, and less than 10 nm roughness. HNA solution can etch the mold isotropically with good uniformity and the smooth surface under the Si_3N_4 mask. The parameters of the HNA etching system mainly determine the uniformity and surface roughness of the molds. In Bai's case, they started HNA isotropic etching at a channel with $200\,\mu m$ width and depth with a 8000 Å thickness thermal SiO_2 buffer layer and a 8000 Å thickness Si_3N_4 mask, as shown in Figure 2.13(d). HNA compositions, temperature, and rotation speed are mainly considered as the key factors to characterize HNA for the molds.
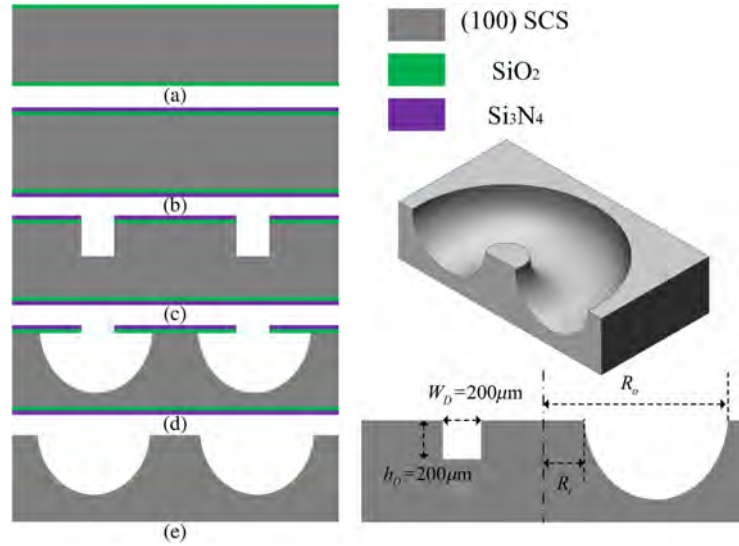
Figure 2.13: Fabrication process of the toroidal molds: (a) thermal SiO_2, (b) LPCVD Si_3N_4,(c)DRIE an annular opening, (d)HNA isotropic etching, and (e) HF cleaning residue [32].

The mask selectivity was investigated in some combinations of different temperatures and HNA compositions under a constant rotation speed of the agitation system. As suggested by Hamzah et al. [49], the volume ratio of HNA was set to (2:7:1), (2.5:7:1), (3:7:1), and (3:6:1) at the right bottom of composition triangle of the HNA composition characterization, because the etching surface smoothness can be guaranteed. Three temperature levels were set to 25 °C, 30 °C and 35 °C and formed 12 sets of experiments for studying the selectivity and etching rate of the mask with the four different compositions in 20 RPM. The selectivity and remaining thickness of Si_3N_4 mask against etchant com-

position at different temperatures were measured when the silicon was etched around $250\,\mu m$ in each experiment, as shown in Figure 2.14. The mask was well kept in relatively high proportion of HF within the range of this experiment setup at $30\,°C$ or $35\,°C$.
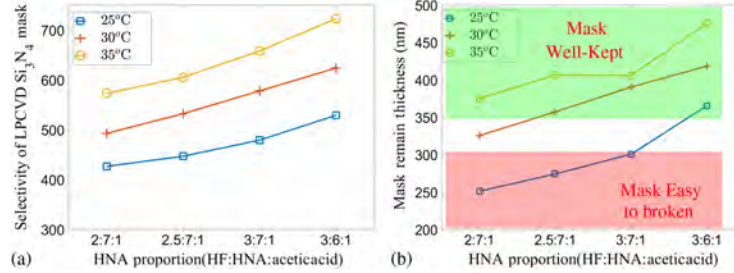
Figure 2.14: Plot of selectivity of LPCVD Si_3N_4 mask and mask remain thickness against HNA compositions at different temperatures in 20 RPM agitation while the silicon is etched about $250\mu m$ [32].

The effect of agitation on etching uniformity and etch rate was also investigated. The rotation setup was built, as shown in Figure 2.15. An agitator with a motor was placed over the solution container to rotate the wafer and solution. Its rotation rate was controlled precisely by the electric motor. The PTFE(Teflon) holder holds the wafer with the shape of a pyramid. The HNA solution was contained by a PTFE bowl. The rotation speeds were set to 0, 15, 20, 25, and 30 RPM. The uniformity and etch rate were calculated or measured.
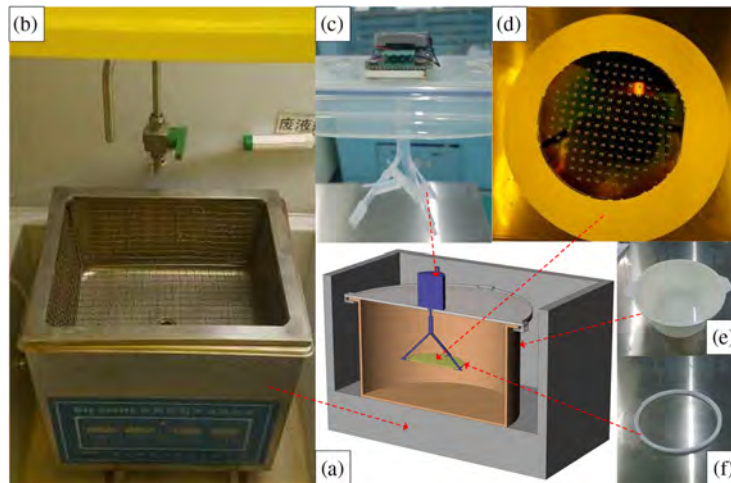
Figure 2.15: Photographs of the wafer-scale etching system. (a) Schematic of etching system, (b) a thermostatic bath supporting ultrasonic agitation, (c) a bracket and a motor, (d) A standard 4 inch, single crystal silicon(100) wafer, (e) a Teflon container and (f) Teflon wafer holder [32].

As Figure 2.16(a) shown, the standard deviation of etching width expresses the etching uniformity inversely. The standard deviation of etching width de-

creases obviously from 0 to 20 RPM and then increases slowly from 25 to 30 RPM. The best uniformity was obtained when the agitation rate is 20 RPM in their experiments.
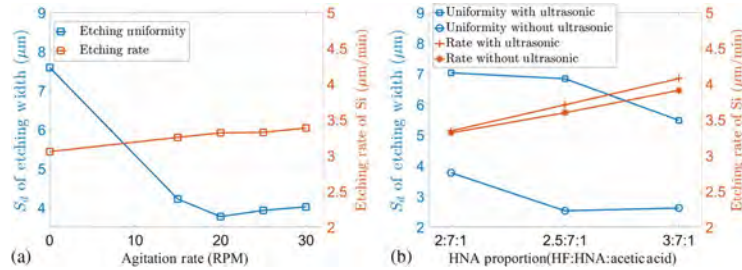

Figure 2.16: (a)Plot of the standard deviation of etching width and etch rate at 30 °C. (b) Plot of the standard deviation of etching width and etch rate against HNA compositions with/without ultrasonic agitation at 30 °C [32].

The result of the temperature effect in the HNA solution is shown in Figure 2.17. It is clear to see that at 30 °C, the hemisphere molds have the best etching uniformity with HNA compositions(2.5:7:1 and 3:7:1) and have no edge hollowed or produce micro holes. With the increase of temperature, the reaction rate is also getting faster within the range of 25 °C to 35 °C, as shown in Figure 2.18.
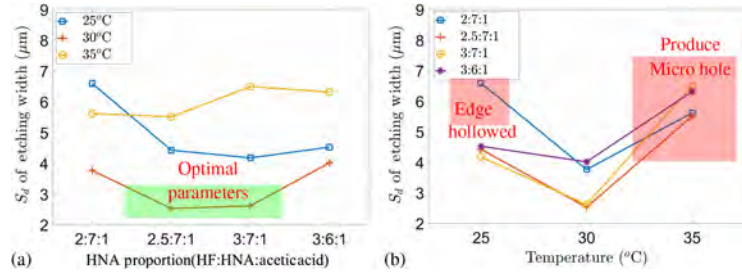
**Figure 2.17:** Plot of the relations between standard deviation of etching width and HNA compositions at three different temperatures [32].
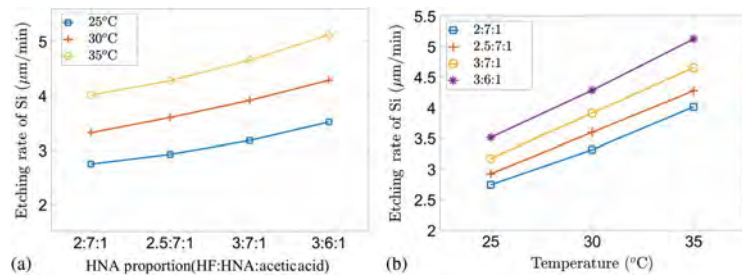
Figure 2.18: Plot of the relations between etching rate of silicon and HNA compositions at three different temperatures [32].

On the premise of ensuring not runaway reaction and smooth surface, appropriately increasing the etching rate is significant for improving the uniformity.

Comparing with HNA compositions 2:7:1 and 3:7:1, the etching rate of the latter increases 24%, and the uniformity improves 34%, calculated from Figure 2.16. The etching rate is equivalent similar at any time of etching, and decreasing the etching time can reduce the cumulative error of etching due to the long-time etching.
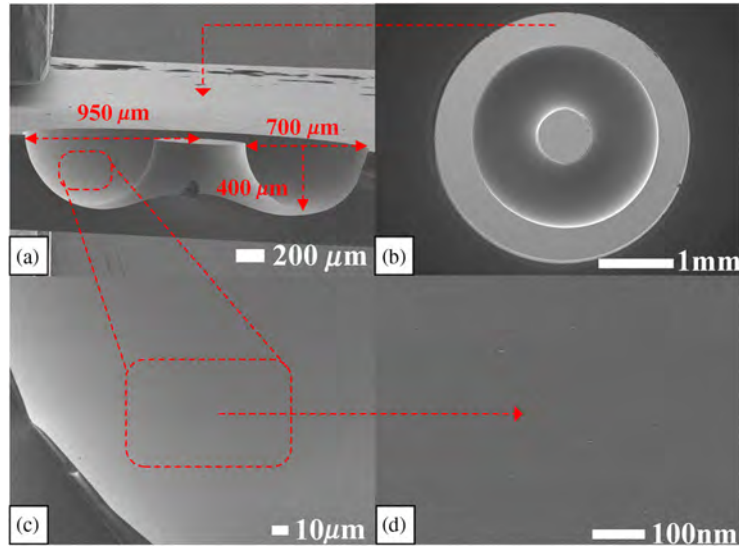

Figure 2.19: (a)SEM image of the cross section of toroidal molds. (b) top view. (c) and (d) are the image of surface of mold [32].

As shown in Figure 2.19, the annular ring size is $700\,\mu m$ in lateral and $400\,\mu m$ in vertical. Since the mold was started from a $200\,\mu m$ width $200\,\mu m$ depth opening, the V/L ratio of etched part is 4:5.

2.3.3   Application 3: deep microchannel

Bauhuber et al. [44] developed that a $300\,\mu m$ deep semi-circular channel with a high optical quality channel wall was produced by isotropic wet etch process for desired light guidance application, as shown in Figure 2.20. In their experiments, three HNA compositions were compared in terms of etching rate, surface roughness, and selectivity in the wet etching process for selecting a best-fitting mixture ratio in beaker experiments. Another etchant, called HNPS(sulphuric and phosphoric acid as diluents), was used to produce smooth and specular surfaces. To further increase the surface quality, a spin etcher that supports solution circulation was used in HNPS wet etching process for producing the channel, and effects of media flux and rotation velocity were investigated in spin-etcher experiments.
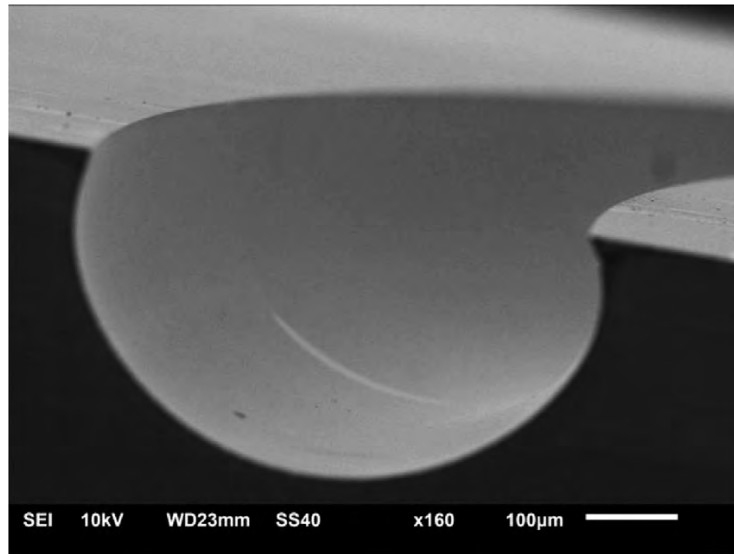
Figure 2.20: SEM image of a $300\,\mu$m deep channel with the channel wall in optical quality [44].

The silicon nitride masked wafer was immersed in three different HNA compositions(in the ratios of (30:60:10), (27:65:8), and (20:70:10)) for characterization. In each beaker experiment, the 250 ml etchant would be replaced by a fresh load after the etching process running for 7 min to prevent the overheating. A magnetic stir bar was placed 20 mm over the wafer with a speed of 60 RPM and was used for providing adequate circulation of etching solution. The etch rates, roughness, and depth for the used etchant was measured, as listed in Table 2.2.

Table 2.2: The measured etch rates, roughness and depth of silicon etched by different HNA compositions in beaker experiments(target depth $100\,\mu$m) [44].

	Original Si	(30:60:10)	(27:65:8)	(20:70:10)
Etch rate (μm/min)	-	16	19	14
Rq (nm)	5	27	19	10
Depth (μm)	0	110	98	105

In their case, the best compositions of HNA are (20:70:10), which has a decent etch rate and good roughness. During the etch process of each 7 min, the solution temperature goes up from 23 °C to 40 °C due to an exothermic reaction. There was dense gas formation occurring, which means that the process was in a runaway or almost. The small gas can stick to the channel surface resulting in the local roughness. Big gas bubbles were restrained by the mask overhangs to partially block the channel surface and lead to wavy channel surfaces. So the temperature instability and bubbles issues are the main factors affecting the inhomogeneity, especially in greater channel depth. Therefore, these influences can be resolved in the spin-etcher process.

The spin etching tool, as shown in Figure 2.21, consists of a medium reser-

voir with a tank capacity of 10 l. The medium was circulated by a membrane pump that supplies the medium dispenser arm. The temperature of the etchant can be kept constant by the thermostat. A filter can block the particle contaminations. The medium dispenser arm moves from the wafer center on a 120 deg circumference segment above the wafer surface according to a given arm speed profile. The etchant can be collected after the flowing across the wafer surface. When the etching process was done, the wafer can be rinsed with DI water and dried with N_2 by other dispenser arms within this system. By this spin system, the etchant temperature was kept 25 °C, the rotation speed were set to 300 RPM, 600 RPM and 1500 RPM.
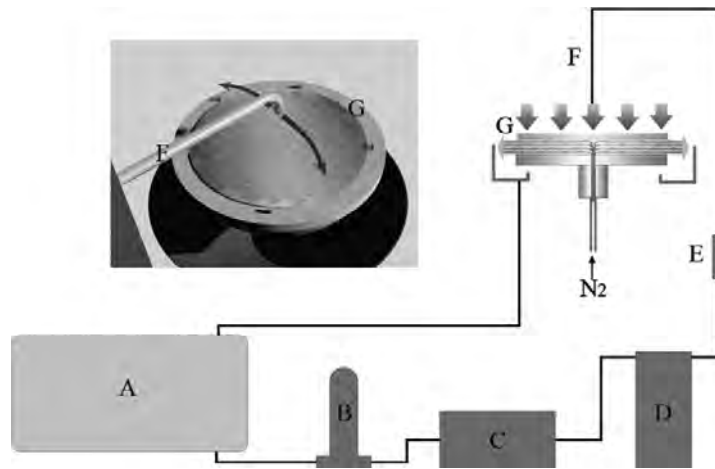
Figure 2.21: Schematic of spin etching tool. (A) reservoir tank, (B) filtration unit,(c) membrane pump, (D)thermostat, (E) flow meter,(F) medium arm, and (G) Bernoulli chuck [44].

The effects of rotation speed influenced the shape of the channel cross-section. As shown in Figure 2.22, at 1500 RPM, it is clear to see the aberration from semi-circular shape. The centrifugal force accelerated the etchant and makes the mask overhangs breaking off, which leads to an inhomogeneous etching result. At 300 RPM, the cross-section is almost perfectly matching to the desirable channel shape.
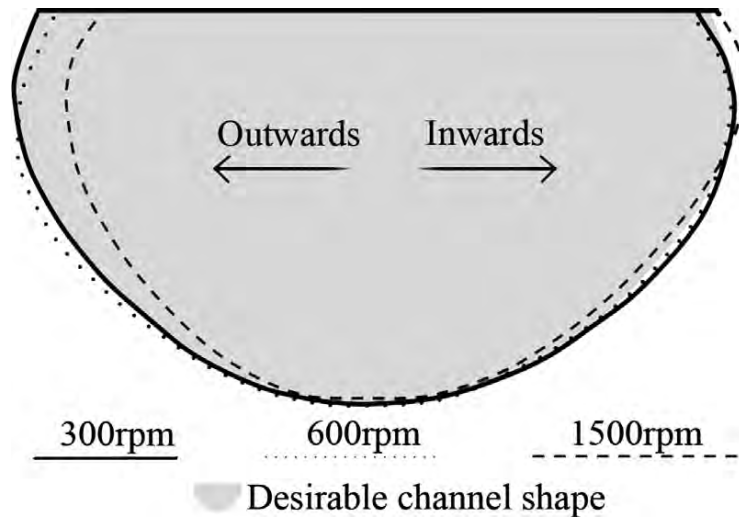
Figure 2.22: Schematic of normalized(scaled to equal channel depth) cross section profile of the etched channel with a depth of $300\,\mu$m with three different rotation speed. The desirable channel shape is indicated in grey fill [44].

This spin-etching setup supports the etchant around the wafer in a circulating way that can maintain the solution temperature, contamination filtering, provide the fresh etching during the process. The roughness and uniformity are performed well on the surface of 300 um deep channel.

2.3.4   Application 4: Wafer thinning

Kim [33] reported a spin-etching method using a configuration in which the silicon wafer rotates in a Teflon bath filled with an HNA solution for the entire wafer thinning. The silicon wafer was rotated at below 60 rpm, where the flow was in the laminar region. Nevertheless, the local etch rate varied with the radial position. Their experimental studies on etch rate and uniformity of etching of 6-inch silicon wafer as the rotational speed was varied were carried out with various HNA mixture ratios.
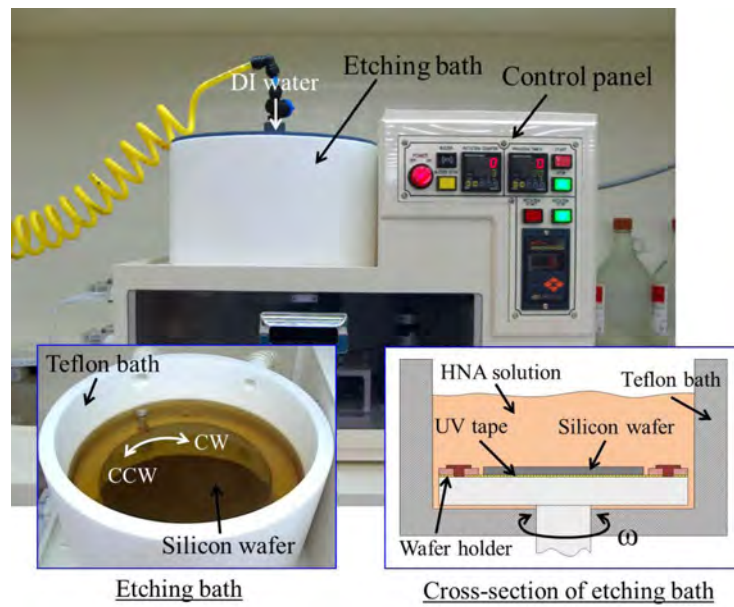
Figure 2.23: Image and schematic of spin-etching system [33].

The spin-etching equipment is shown in Figure 2.23. The wafer holder was rotated by a servo-motor system with a rotational speed control system. The 6-inch silicon wafer, which is protected by UV tape, was mounted on the wafer holder. After the spin-etching test, the thickness of the nine points on the wafer was measured. One point is at the center, four are located at 30 mm far away from the center, and another four are located 60 mm from the center. The thickness differences between before and after etching were measured by depth gauge to calculate the uniformity and etch rate. The HNA compositions were 1:4:3, 3:5:3, and 35:45:20, where the concentration of CH_3COOH is 80wt% for these experiments. The agitation speed was set to 0 RPM, 15 RPM, 30 RPM and 60 RPM, and the rotational direction changed when every ten rotations finished.
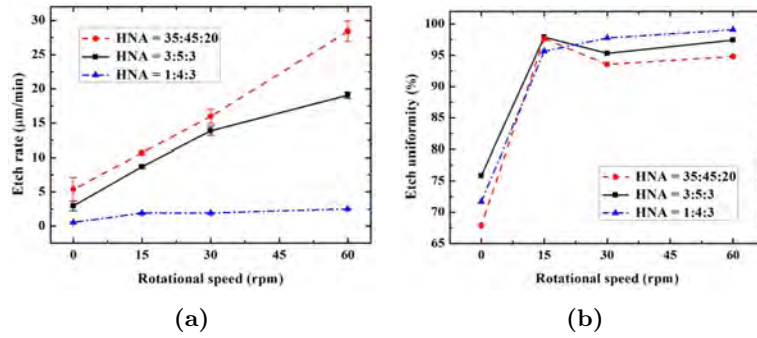
Figure 2.24: (a) Plot of etch rate as a function of rotational speed in different compositions with 10 rotations in each rotational direction. (b) Plot of uniformity against rotational speed in different compositions with 10 rotations in each rotational direction [33].

The etch rate and uniformity as a function of rotation speed are shown in Figure 2.24. With an increase in rotation speed, the etch rate is increasing with the composition dependency. The uniformity is increasing from 0 to 15 RPM, but it does not vary when the rotation speed is greater than 15 RPM.

This paper described a way that rotates wafer in relatively pure rotating motion without any additional stirring by a braced structure in wafer holder, as mentioned in previous articles, supporting a laminar environment in the etching process. However, HNA in the wet etching process is a temperature dependency system. It has a high possibility that runaway reaction occurs without any temperature control, especially dip the entire maskless silicon wafer in the etchant in their experiments. It is worth noting that the direction of rotation ran clockwise and counterclockwise every ten rotations alternatively. It might help improve the symmetry of the corner structure.

2.3.5   Summary

HNA system can be used in different applications by modifying the etching parameters(compositions, temperature, rotation speed, Etc.), which is already reviewed in this section. The preparation of each mentioned application is listed in Table B.1. The column etching location indicates the depth of the starting point of the wet etching process under the front surface of the silicon layer of the wafer. Window width indicates the pattern of mask or distance between two adjacent microstructures. The etching parameters and evaluations for each mentioned application are summarized in Table B.2. The HNA compositions around (2:7:1) are popular. It locates at the right bottom of the composition triangle and gives a decent etch rate and roughness, and with proper agitation, the uniformity increased. Because the majority selected composition is at the high HNO_3 concentration, the activation energy of the reaction is not high. Maintaining the temperature at around 30 °C is the right choice. Not only can it prevent the runaway solution, but also the etch rate increases. Decreasing the reaction time reduces the cumulative error of etching. The parameters and results of these examples provide partial information that would help to etch

the buried channel.

2.4   Conclusion

This chapter introduces the theory of HNA systems and reviews some published papers relating to application etched by HNA etchant. Many factors affect etching performance, such as temperature, the rotation speed of solution, HNA composition, Etc.

Temperature affects the reaction between HNA solution and silicon. If the temperature is too low, the reaction can not happen. If the temperature is too high, the etch rates on the vertical and horizontal directions are different, and the runaway reaction should be considered. The isotropic etching happens at the temperature interval between $20\,^\circ$C and $35\,^\circ$C at the low HF and high HNO_3 composition regions.

The stirring or rotation system is essential to get a decent etching performance in the HNA system. The compounds should be well mixed in the etchant solution. Otherwise, the uniformity on the wafer is affected. The different microstructure needs different rotation rates and wafer orientation. The microneedle arrays seem to need high stir speed, and the hemisphere structure needs a gentle rotation speed.

HNA compositions not only affect the etch rate, but also the surface roughness. The compositions at low HF and high HNO_3 have the lower activation energy, perform a faster etch rate, and a smoother surface than the high HF region. For a long-term etching process, the thickness of the mask layer defines the etching period. The mask still can be etched by the etchant, notwithstanding Si_3N_4 has a very low etch rate comparing to the silicon. Additional SiO_2 could be deposited on the Si_3N_4 layer to extend the etching time to achieve a larger cavity, but will consume the HF at the beginning.

For achieving etching a big tube underneath the silicon wafer, the etch parameters of the mold structure can be selected. The microtubes are etched by the HNA compositions in a ratio of 2:7:1 in room temperature with a rotation speed of around 20 RPM.

Chapter 3

Etching bath in HNA system

Based on the preceding theory and those applications' etching parameters, the HNA solution with a rotation system is a way to have a proper wet isotropic etching. A etching bath with rotation system is designed. Due to the strong corrosive and toxic, the etching bath made of standard material can not survive in this mixed solution, and operational safety during the experiments should be considered. In this chapter, the material selection, design idea, structure, and standard operation process of a customized etch bath are introduced.

3.1   Introduction

Generally, the quick operation steps of the wet etching processes can be summarized as:

1. Prepare the etchant.

2. Immerse the wafer in the solution.

3. Rotate the wafer carrier.

4. After wet etching, take out the wafer and rinse the wafer in the quick dump rinse tank.

   However, in practice, some etchants are dangerous to researchers. An etching bath is designed to rotate a wafer in the HNA solution with a constant speed for increasing the uniformity of big tubes underneath the wafer. The wafer should always be rotated in a unique motion during the long wet etching process. Additionally, all experiments with respect to the HNA solution proceed on the wet bench in the cleanroom, so the etching bath's operability and operational safety should meet the requirement to make the etching bath as an external device allowing to be introduced in the cleanroom. Therefore, the design requirements are listed:

- The wafer is only rotated in Rz direction(see Figure 3.2), and other degrees of freedom(DOFs) are constrained during the experiment.

- The wafer is rotated at a constant speed during the experiment.

- The entire etching bath is designed for anti-corrosion.

- Any metal component or element of the etching bath is not exposed to the wet bench.

- The wafer should only be operated/driven by specific tools.

3.2   Etching bath design

The etching bath mainly consists of three parts, the fixed frame, the movable rotation system, and a detachable wafer carrier. The overview of the etching bath is shown in Figure 3.1. The fixed frame is supporting the entire structure to prevent toppling. The movable part translates along the guide axis to start or stop etching. The wafer carrier is a module design that could simplify the operation steps and thus ensure safety.
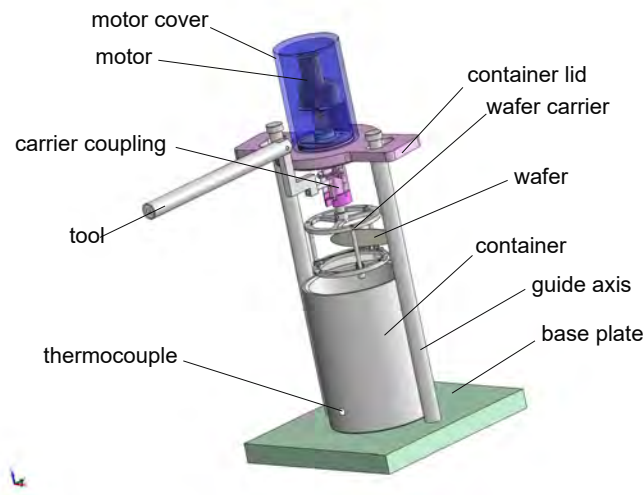
Figure 3.1: Overview of etching bath. The fixed frame consists of the base plate, two guide axes, and the container(Actually, the container is detachable. Due to its weight, it is not easy to take out from the base plate.) The pink and blue parts indicate the movable rotation system. The wafer carrier is a detachable part so that it can be easily assembled to/ disassembled from the movable part.

3.2.1   Material selection of main body

The first point that should be considered for the etching bath material is the chemical resistance against both hydrofluoric acid and nitric acid. Polytetrafluoroethylene(PTFE), Perfluoroalkoxy alkane(PFA), Fluorinated ethylene propylene(FEP), and Polyvinylidene fluoride(PVDF) can be chosen since they can

survive in HNA solution within the temperature range of experiments[1].

Table 3.1: Mechanical properties of four fluoropolymers [52].

|	PTFE	PVDF	PFA	FEP
Density(kg/m^3)	2140-2200	1780	2150	2150
Flexural Modulus(MPa)	620	1600	690	660
Hardness	55-72	73-85	60-65	55-60

The majority of the materials used for this design are PTFE and PVDF. Both materials have good resistance against HF(50 wt.%) and HNO_3(69 wt.%) at the operating temperature range of this wet etching processing. As can be seen from Table 3.1, PVDF has higher hardness and flexural modulus than others. Therefore all components designed for structural brace are made of PVDF. Other components are made of PTFE due to the lower price.

The base plate, container, container lid, glide ring, and motor cover are made of PTFE. The guide axis, carrier coupling, wafer carrier, excenter, tools, close-off ring, and some insert pins for the joints are made of PVDF. Other elements have to be made of metal due to the greater hardness, but they are protected by PTFE. The motor clamp bushing is made of Ms58(a cooper-zinc-lead alloy), and the motor lid connection is made of RVS316(stainless steel).

3.2.2   Core design

The design's core is making the wafer rotating in Rz-direction and constraining the rest during the etching process in the entire etching bath system. The main idea is based on the 1-DOF rotational mode [53], as shown in Figure 3.2.

---

[1]Some of these polymers surrender at a higher temperature in HNO_3.
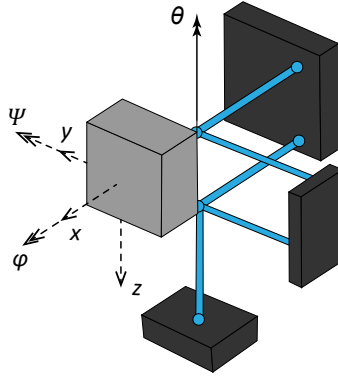
Figure 3.2: Schematic of the 1-DOF model. The blocks in black represent the anchors. The rods in blue are considered as rigid bodies, which cannot be bent, elongated, or shortened. The blue balls attached to the rods are also rigid bodies allowing the rods rotating. The block in grey stands for the wafer in the etching bath during the etching process, which only rotates perpendicular to the z-axis(θ). Double arrows and single arrow signs mean the rotation and translation motions, respectively. Dash lines mean constraining, and solid line means free motion.

Wafer carrier

The wafer carrier plays three roles in the etching bath. First of all, it constrains a 4-inch wafer. The wafer should be fully constrained in the wafer carrier before rotating in the etching bath. Otherwise, it will float randomly in the solution during the etch process. The wafer carrier is designed like a cage, as shown in Figure 3.3. The wafer(shown in blue) lays on the wafer carrier ring. The wafer carrier ring has a 1 mm sink as a shape of a 4-inch wafer. Therefore, the wafer can not translate in the XY-plane, and the primary flat edge constrains its Rz-direction motion. The three clamps attached on carrier rods limit the wafer moving up, pitch and roll when the wafer carrier is pressed in the solution. Thus the wafer is fixed in a wafer carrier. The grey transparent wafer indicates the way to insert the wafer into the cage along the diagonal of any two carrier rods. For saving space, the height of the cage is the diameter of a 4-inch wafer.
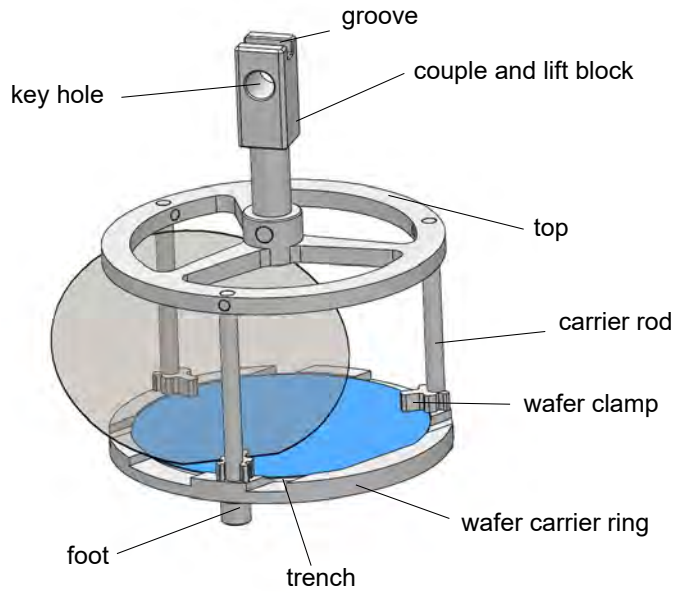
Figure 3.3: Schematic of the wafer carrier.

Secondly, the carrier and wafer as a one-piece are driven by a motor. The coupling will be well explained in the next part of this subsection.

Finally, after the etching process, the wafer carrier should be sent to the quick dump rinse(QDR) as soon as possible because the residual solution can still etch silicon. The trenches on the wafer carrier ring are designed to let the bottom air out when the wafer is pressed into the solution. They also make a highway to let the deionized(DI) water pass by the wafer to decrease the rinse time in the QDR, and the three feet do as well.

Carrier coupling

Carrier coupling is the transmission shaft between the wafer carrier and the motor, as shown in Figure 3.4, acting fixation on the lift block of the wafer carrier. There is also some space leaving for rotating the excenter. The excenter can be driven by a T-shape tool, as shown in Figure 3.5. Thus its arm can rotate to the groove of the wafer carrier for constraining the carrier. When the arm is rotated to other angles, the lift block can be inserted in or pulled out by using a Z-shape tool via the keyhole.
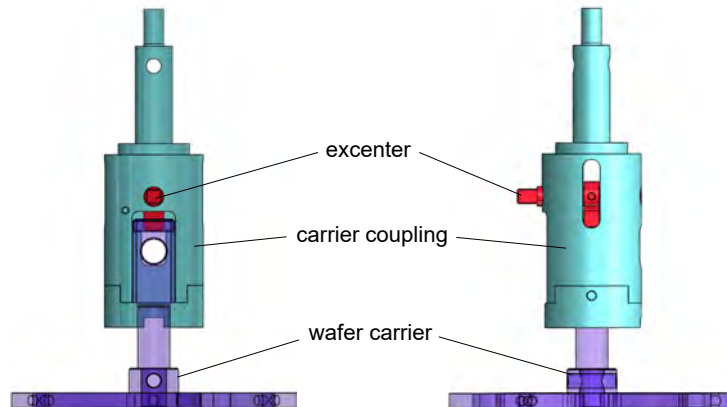
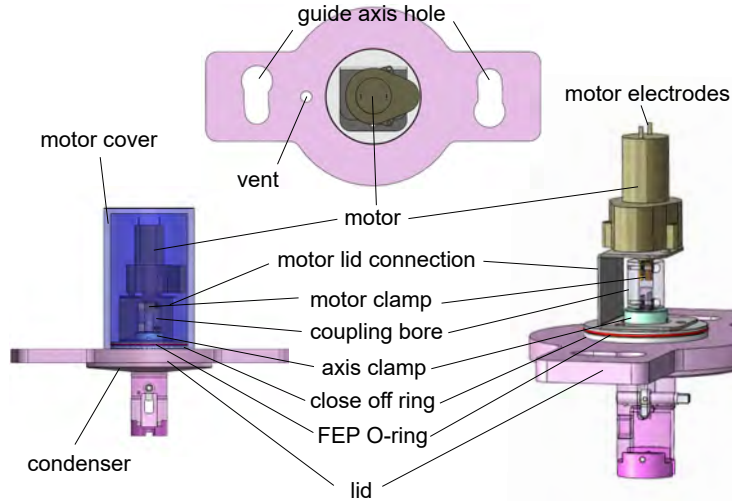**Figure 3.4:** Side views of the carrier coupling.
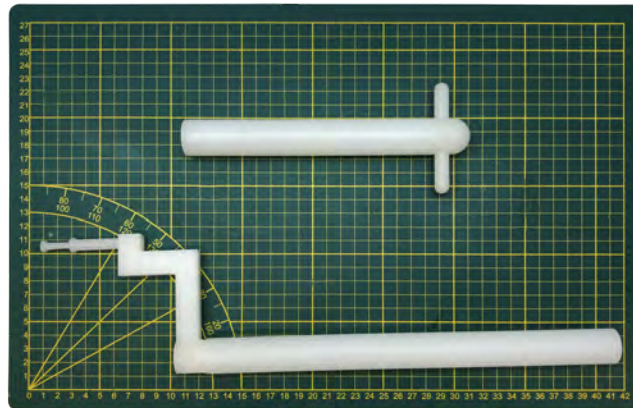
Figure 3.5: Accessories of etch bath. Top: T-shaped tool ; Bottom: Z-shaped tool.

Container lid

The container lid is the most massive movable piece in the etching bath, as shown in Figure 3.6. It consists of two parts. One is the lid, which acts on a platform for the rotation unit and wafer carrier unit. The lid can move up and down along the two cylindrical guide axes. When the lid moves to the top and rotates a certain angle, the whole part will be stuck at the top of the guide axes for the operator to place or remove the wafer carrier by the tools. When the lid moves to the top of the container, the wafer carrier ring can be immersed in a solution(462 mL). Under the lid, there is a condenser that right closes the container. This condenser mainly cools the gas down resulting in backflow. The vent on the lid is designed for reducing the pressure difference inside or outside
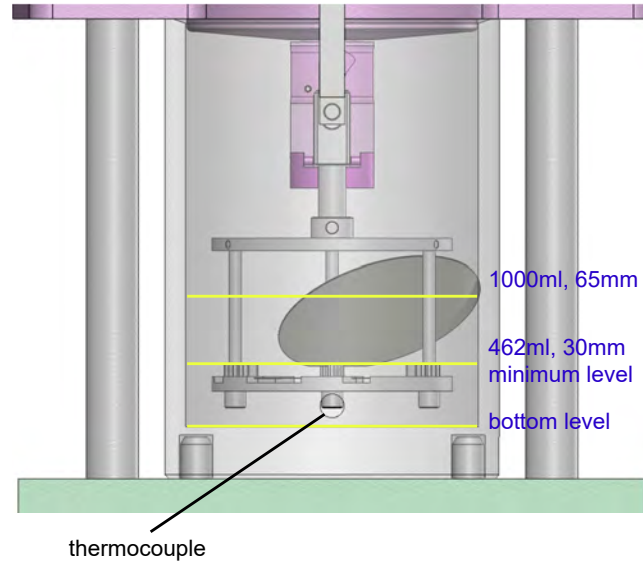
of the container.

Figure 3.6: Three views of container lid.

Above the lid, the rotation system is protected by the motor cover. A motor is supported and fixed by the motor lid connection. There is a motor coupling placing between the motor axis and the top of the carrier coupling. Thus even if the motor and carrier coupling is directly connected and correctly fixed, slight misalignment can occur over time due to changes in temperature and changes over a long period of time, causing vibration and damage. The motor coupling acts on a vital link to minimize impact and vibration, allowing smooth rotation to be transmitted. An AC/DC power supply drives the motor. According to the rotation rate measurements, the motor can drive the wafer carrier in 10 RPM, 25 RPM and 40 RPM with 5 V, 10 V and 15 V that are marked on the supply, respectively.

Container

As shown in Figure 3.7, the container sits in a round pit on the base plate, and there are also two press pins inserting in the bottom of the container to prevent toppling over. A slope structure on the container's opening prevents the liquid from pouring out when the lid rises. The container's inner height is 192 mm and its inner diameter is 140 mm. The liquid level of 1 L solution in the container in around 65 mm. For just covering the wafer when the wafer carrier is dropped in, the minimum volume of solution is 462 mL. Due to the safety, the container has a 20 mm thickness wall for keeping the mass center low and preventing toppling, which is difficulty to heat the etchant from outside because the PTFE has low thermal conductivity.

Figure 3.7: Cross-section view of container when the lid is closed. The solid yellow lines indicate the liquid levels in the container. The thermocouple hole is on the container wall, which is for inserting the PTFE-coated thermocouple to the etchant. The thermocouple and hole are fasten by a screw so that prevent the leakage.

A PTFE-coated thermocouple can insert via the hole on the container wall. Thus, the solution's temperature can be measured, but the readout response is slow due to the bad heat conduction of PTFE.

3.2.3 Standard operational processes

To safely work with this etching bath in the cleanroom, the designers make the standard operational processes to etch a wafer with a rotation system on the wet bench. This part explains the operating details and reasons.

On the whole, the etching bath can be split into two parts - inside and outside of the wet bench in operation. The devices inside the wet bench must be operated by wearing the chemical resistant gloves, especially when the solution consists of HF and HNO_3. The only device outside the wet bench is the power supply for the motor. The power supply has an on-off-(on) switch that allows the motor to rotate in the toggled mode for a long term or held-on mode for fine-tuning the excenter towards the front(convenient to move the wafer carrier).
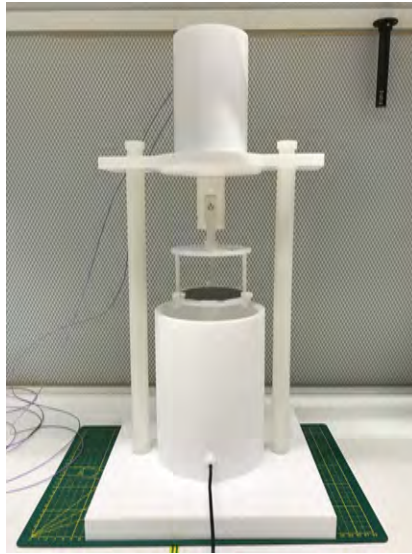
Figure 3.8: Image of etching bath in idle state.

In the beginning, the lid should be locked on the top-end of the guide axis, as shown in Figure 3.8. If not, the operator can hold the lid's ears, rise up to the highest level, and rotate clockwise a little bit to the lock position by both hands. Thus the guide axis holes(middle of Figure 3.6) can be stuck at a ring-shaped groove. When the excenter towards the front, using a T-shaped tool can quickly turn the excenter inside the carrier coupling(see Figure 3.9). To take out the wafer carrier, the operator can insert the Z-shaped tool's tip into the wafer carrier's keyhole and pull it up a little to take out.
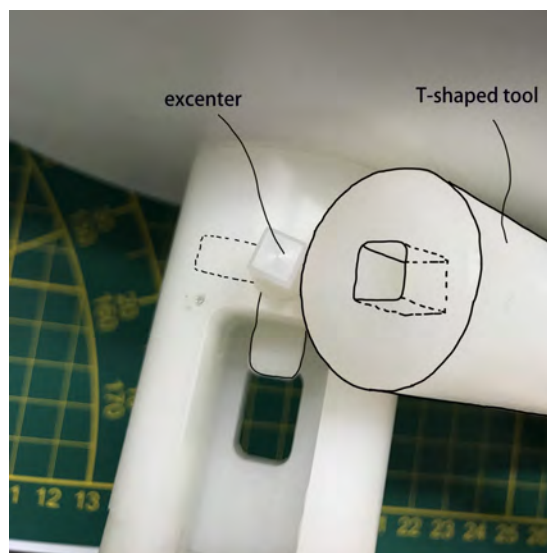
Figure 3.9: Image of excenter and rectangular hole of T-shaped tool.

The next step is loading the wafer into the carrier. Rotate the three wafer clamps to the outside and hold the primary flat of the wafer by tweezers. Insert the wafer at a certain angle(see Figure 3.10) between any two rods and make sure the primary flat edge aligns with the flat side of the wafer carrier ring. Finally, rotate the clamps inside to fix the wafer.
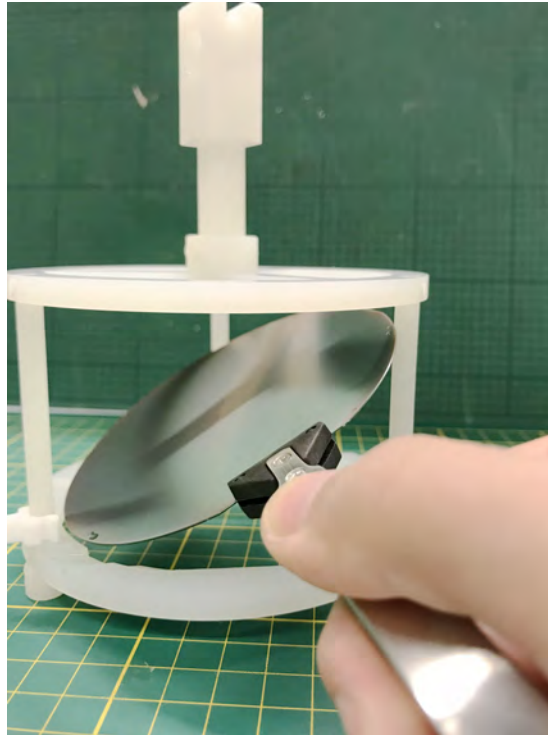
Figure 3.10: Insert the wafer into the wafer carrier.

Put the wafer carrier back to the carrier coupling by the Z-shaped tool. Rotate the excenter down to lock the carrier. Then the prepared solution can be poured into the container. Switch the motor on the toggled mode. Hold the lid ears by hands with chemical resistant gloves. Rise the lid up and rotate it anticlockwise to unlock the guide axes and gently drop the lid down on the container. Rinse the tools with DI water.

After wet etching, the wafer carrier should be moved to QDR as soon as possible because the etchant is attached to the etching surface, especially for the buried channel etching. Repeat the carrier taking-out steps and move the wafer carrier with wafer into the QDR tank directly. Rinse the platform and tools with DI water.

3.3 Modular design

The customized etching bath is a modular design. Some parts of the etching bath can be redesigned, upgraded, repaired, and reused for different purposes.

The modular design is allowed to expand for efficient etching, such as modeling a new wafer carrier that can carry more wafers and etch them together in one round process. The container can also be modified by adding the hot wires around the wall driven by a power source to heat the etchant and design a build-in PVDF(-coated) piezoactuator to generate ultrasonic in the etchant. Alternatively, the container part can be replaced by an ultrasonic bath with a temperature controller. However, here these ideas list that have not been realized yet.

3.4 Conclusion

This chapter elaborates on the design concepts, material selection, structure, operation process, and modular expansion of the customized etching bath, which is a reliable, stable rotational system developed for the wafer in the isotropic wet etching process. The customized etching bath is designed for meeting the safety requirements of the cleanroom, ease of operation, and further updates.

Chapter 4

# Experimental Setup

4.1 Introduction

The experiments are established based on the theories and published information, as mentioned in Chapter 2. In this chapter, fabrication processes before wet etching and patterns are introduced first. The experiment setup then describes that the well-prepared wafers are etched by HNA solution in various HNA compositions and rotation speed. Finally, etched structures are surveyed from three views in the observation method and analyze depending on the results.

4.2 Fabrication Processes

For characterizing the HNA solution effecting on the different structures on the surface of the wafer or underneath, two fabrication processes are introduced until the wet isotropic etching. The mask layer for both processes is SiRN, due to the higher selectivity of SiRN than SiO_2.

4.2.1 Process flow(a) - surface

a) A 100 mm diameter, 525 μm thickness, p-type, double sides polished single crystal silicon $\langle 100 \rangle$ wafer with a resistivity of 5 Ωcm to 10 Ωcm is used as substrates.

b) A 1000 nm low-stress SiRN is deposited as the wet isotropic etching mask by low pressure chemical vapor deposition(LPCVD).

c) The lithography defines a 10 μm width channels pattern (or 10 μm diameter dots pattern). Etch the unprotected SiRN by plasma etching.

d) HNA wet etch.
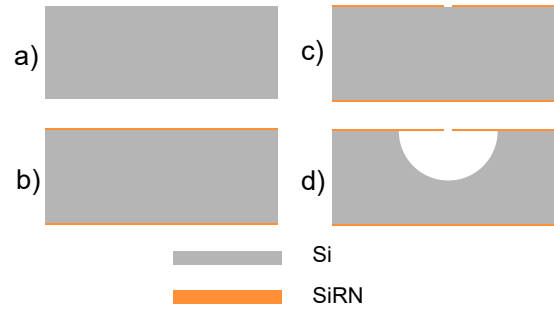
Figure 4.1: Process steps used to fabricate the dot/slit test until wet etching process.

4.2.2   Process flow(b) - buried

A schematic of the process steps used to create the buried channel is shown in Figure 4.2.

a) A 100 mm diameter, 525 μm thickness, p-type, double sides polished single crystal silicon $\langle 100 \rangle$ wafer with a resistivity of 5 Ωcm to 10 Ωcm is used as the substrate.

b) A 500 nm thermal SiO_2 is grown on the silicon at the 1150 °C as the mask layer for the following plasma etching process.

c) The lithography defines a 10 μm width channel pattern. Then unprotected SiO_2 is removed by directional reactive ion etching.

d) The silicon channel opening is etched downward 65 μm by the Bosch process.

e) All SiO_2 layer on the wafer is removed by 50% HF solution.

f) A 1000 nm low-stress SiRN is deposited as the wet isotropic etching mask by low pressure chemical vapor deposition(LPCVD).

g) A 2000 nm SiO_2 layer is deposited as a mask layer for protecting SiRN.

h) Etch the multilayers of SiO_2 and SiRN by plasma etching.

i) HNA wet etch.

In step(c), the unmasked SiO_2 layer is overetched 100% for perfect pattern transfer, and it ensures that the DRIE process can start to etch the silicon. In step(g), the SiO_2 is deposited by PECVD on the SiRN layer at the surface of the wafer. The SiRN at the trench bottom will not be covered by SiO_2 due to the trench's high aspect ratio with a small window. Therefore, the SiRN was removed by plasma etching in step(h), and the SiRN on the surface was remaining. Alike, the bottom is also overetched, so that the bottom is fully opened.
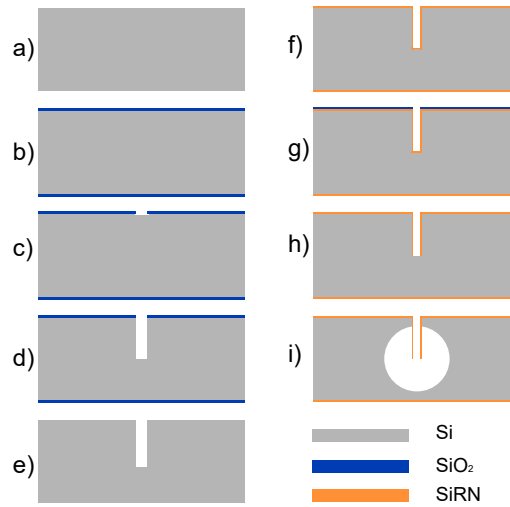
Figure 4.2: Process steps used to fabricate the buried channels until wet etching process.

4.3 Patterns

Three patterns, as shown in Figure 4.3, are used for these experiments. Naturally, the dots pattern is only for comparing the uniformity over the whole wafer, whether the rotation system is applied. The long slits pattern can be used either in the surface channel processing or in the buried channel processing for showing the uniformity and etching result with the different HNA compositions. The first sub-figure shows that 169 dots with a diameter of $10\,\mu$m are placed as a hexagon in a 4-inch wafer. The distance between any two adjacent dots is $5\,$mm. Second, 11 long slits with the $10\,\mu$m width are arranged in parallel with a $6\,$mm gap between two neighboring slits. The last one is the pattern of Coriolis shape devices in small differences. Compared to the slits pattern for buried channel technology, the Coriolis shape has less microloading and less window for etchant transfer.
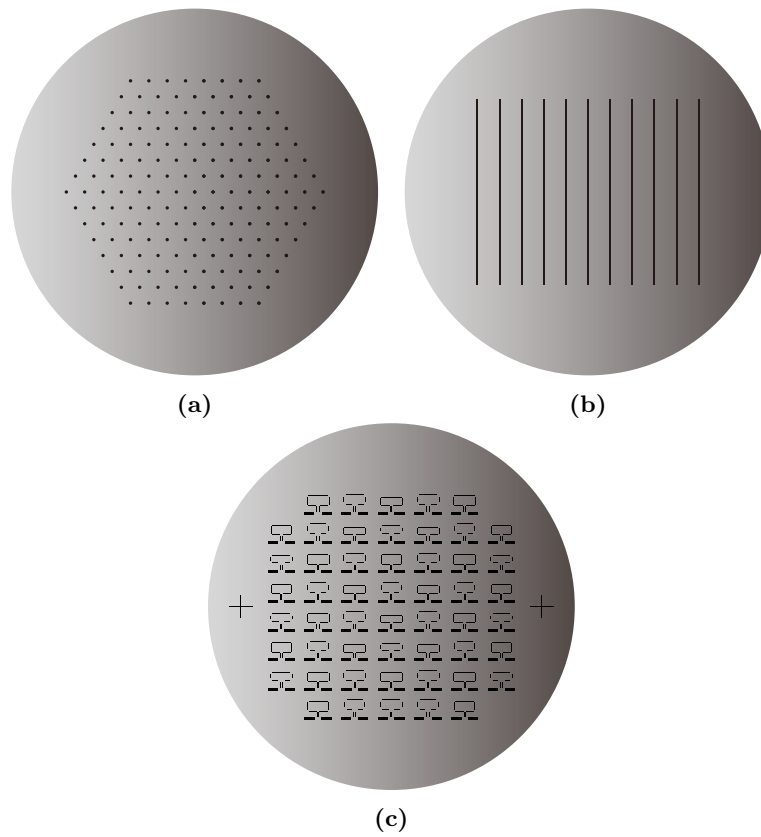
Figure 4.3: Patterns of 169 dots(a), 11 slits(b) and Coriolis shape(c).

4.4   Experimental plan

All experiments were done at 20 °C, because the container wall of etching bath is too thick to heat because of the bad thermal conductivity of PTFE. In experiments A and C, the wafer was put in a PTFE vessel with 200 mL HNA solution. The wafer was carried and rotated by the etching bath with one liter HNA solution for the rest experiments. The specific etching parameter are listed in Table 4.1.

<div align="center">

Table 4.1: Table of the experimental setups

</div>

ID	Pattern	Process flow	HNA Compositions[1]	Rotation (RPM)	Etching time(min)
A	Dots	(a)	2:7:1	0	40
B	Dots	(a)	2:7:1	25	40
C	Slits	(a)	2:7:1	0	40
D	Slits	(a)	2:7:1	25	40
E	Slits	(b)	2:7:1	25	90
F	Slits	(b)	3:6:1	10	90

[1] Volume ratio of HF(49 wt%), HNO_3(69 wt%) and CH_3COOH(99 wt%).

## 4.5   Observation methods

4.5.1   Optical Microscopes

The optical microscopes are used for observing a large number of samples in the whole wafer because of high efficiency and straightforward operation. The test structures are observed by the optical microscope under the 50x objective lens through a 10x eyes lens on the probe station and captured by the build-in Nikon J4 digital camera. The size of photos is set to 5232×3488 (18.2 MegaPixel). After the calibration, $100\,\mu$m is equal to 1990 Pixels in the picture. Therefore, the scale is set to $19.9\,\text{pixel}/\mu$m for measuring.

Top view   The images are post-processed for improving the quality, especially for a clear edge, before counting the pixels. As shown in Figure 4.4a, the greenish is an exciting area to be measured for dots test: The image is sharpened to a certain level that can distinguish the edge. Create a mask to define the areas in high contrast colors by the edge. Select the area within the edge by wand tool. Measure the greenish area in width, height, and circularity and then return the data for analysis. The dots' vertical distance is defined as the length from the highest pixel of edge to the lowest and the major axis for horizontal distance. The circularity is defined as

$$\text{Circ} = \frac{4\pi A}{S^2} \tag{4.1}$$

Where A indicates the area of selection, and S is the perimeter. A value of 1.0 in circularity indicates a perfect circle. For the long surface channels, as shown in Figure 4.4b, the width of the greenish area is measured: Switch on the grid in the window of ImageJ and rotate the image to a certain angle that connects the vertical edge to the grid. Use the rectangular tool to select the channel. Measure the width of the surface channel.

(a)   (b)
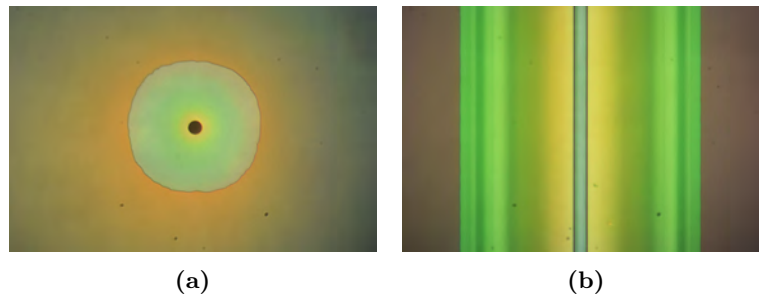
Figure 4.4: Top view of the dot(a) and the long surface channel(b) in the wafer under the optical microscope. The greenish indicates the underetch under SiRN mask. The slit at the center is the window etched by RIE and also indicates the specular surface at the bottom of channel. The black dot indicates the non-specular surface at the bottom.
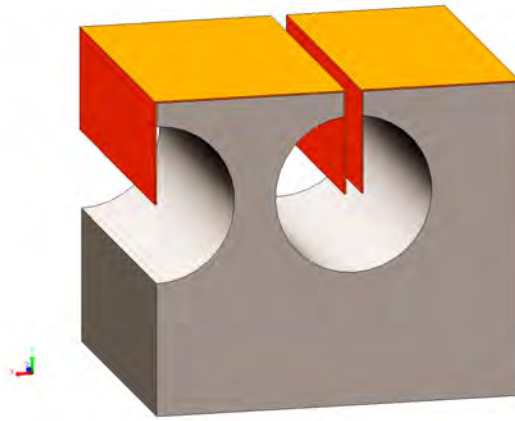

Figure 4.5: The buried channel can be observed in lengthwise-section view and cross-section view.

Cross-section view   Observing the cross-section(Figure 4.6) of the channel is a way to the quality of underetching. The diameters of surface or buried channels can be seen in this view. Since the channels are perpendicular to the primary flat edge in the ⟨100⟩ wafer, the channels can be easily broken off into several slits when the edge of the wafer is scratched.

<div align="center">(a)   (b)</div>
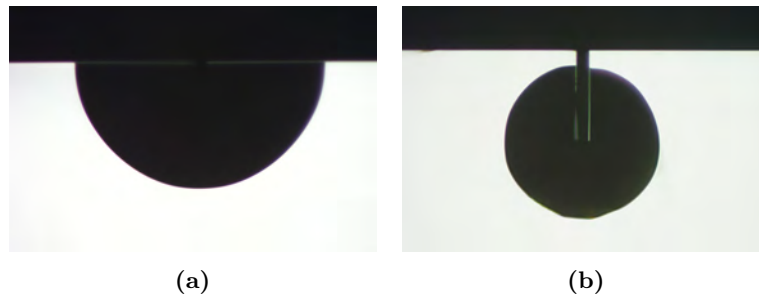
Figure 4.6: Optical microscope photographs of cross-sections of the long surface channel(a) and the buried channel(b).

Lengthwise-section view along the channel   The channel's diameter and roughness can be observed through the lengthwise-section along the channel, as shown in Figure 4.7, for example. Unlike the cross-section, lengthwise-section shows the etching result, especially the roughness, continuously along the channel.
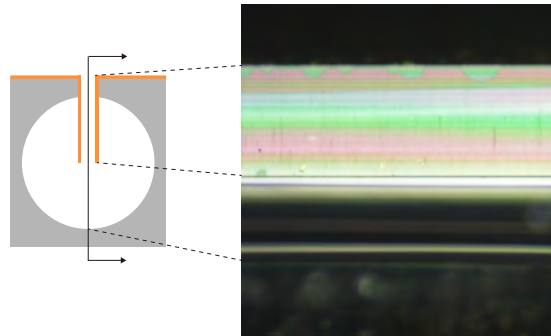
Figure 4.7: Left: Schematic of observation direction. Right: Lengthwise-section view along the channel of a smooth inner wall of a buried channel observed by optical microscopes. The colorful rectangular is the SiRN sidewall.

4.5.2 Observation errors and failures from optical microscope

The light cannot pass through the sample for a reflected optical microscope because the sample surface reflects it, eventually returned and detected by the camera or eyes through the microscope lens. Therefore, some errors might affect measurement accuracy, as listed below:

1. Tilt angle of the sample surface. The surface of the sample in the holder can not be placed parallel to the object lens perfectly. It will result in that one spot is focused, and the rest is out of focus, especially in the high magnification.

2. Breaking wafer. The samples are broken off easily when the diamond knife scratches the edge for observing the cross-section. The dicing saw was not used because it would create a coarse surface. Sometimes the cross-section

containing the buried channels has different fracture levels resulting in a focusing problem.

3. Vibration. In high magnification, the image would be blurred due to the shake when pressing the shutter button. The shutter with a timer could cancel this effect.

4. Selection in ImageJ. It is hard to determine the blurred edges affected by the shake, and out of focus in the image, even the image has been sharpened.

Chapter 5

Results and discussion

This chapter will discuss the results in terms of the experiments from Table 4.1.

5.1 Rotation system tests

According to the applications in Section 2.3, the rotation system can improve the uniformity of devices in the wafer during HNA etching. The dots and slits experiments show that the apparent improvement of uniformity.

5.1.1 Dot experiments

Experiment A The well-prepared dots sample wafer was immersed statically in 200 mL HNA solution with 2:7:1 composition at room temperature and etched for 40 min. The sample dots are observed by an optical microscope and captured by the built-in camera. The images are processed by the software ImageJ to obtain the edge of cavities under the SiRN layer. The vertical and horizontal distribution of sample dots in one wafer is plotted in Figures 5.1 and 5.2, respectively. Dots with a larger vertical or horizontal diameter than the mean value of sample columns are marked by the red plus sign in each plot. According to these two figures, the dots with the dimension below the mean value gather at the bottom left zone. The standard deviation of vertical and horizontal diameter is $1.32\,\mu$m and $1.35\,\mu$m, respectively.
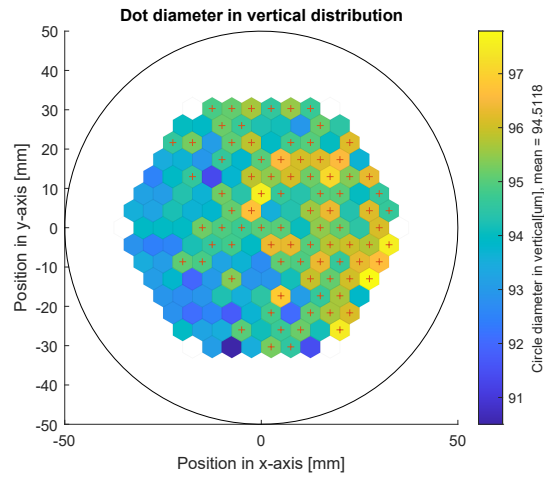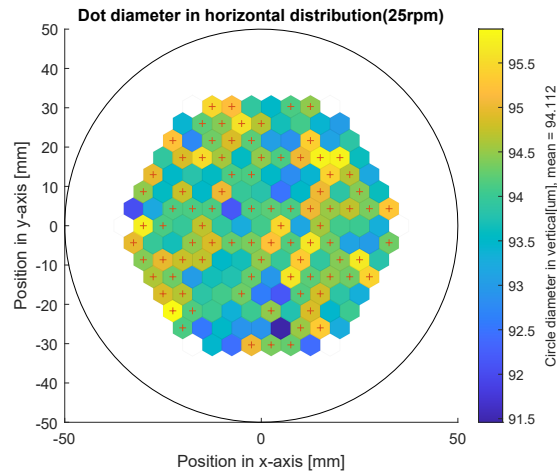
Figure 5.1: Plot of dots' vertical diameter distribution in a wafer. Plus signs indicate the height larger than median value of sample dots. HNA = 2:7:1, Etch time = 40 min, Rotation = 0 RPM.
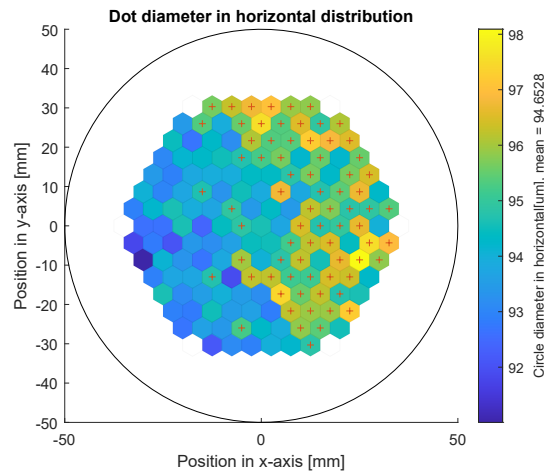
Figure 5.2: Plot of dots' horizontal diameter distribution in same wafer. Plus signs indicate the width larger than median value of sample dots. HNA = 2:7:1, Etch time = 40 min, Rotation = 0 RPM.

Experiment B   Figures 5.3 and 5.4 show that the distribution of the dots on the wafer while the wafer is rotated at 25 RPM in a one-liter etchant. As can be seen from the figures, the mean value is similar to the result without rotation, but dots with the dimension higher than the mean value intersperse among the wafer. The standard deviation of size is reduced from 1.32 to 0.84 for vertical diameter and from 1.35 to 0.87 for horizontal. Therefore, the agitation system has a positive effect on the dots test. The top view of all dots looks like Figure 4.4a. The central point is black, which means that the bottom is not specular.

Figure 5.3: Plot of dots' vertical diameter distribution in a wafer. Plus signs indicate the height larger than median value of sample dots. HNA = 2:7:1, Etch time = 40 min, Rotation = 25 RPM.
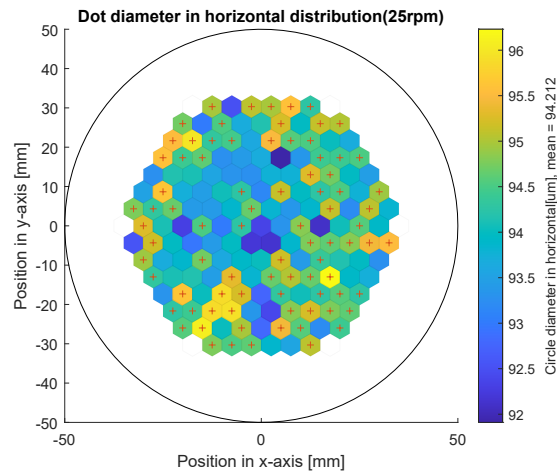

Figure 5.4: Plot of dots' horizontal diameter distribution in same wafer. Plus signs indicate the width larger than median value of sample dots. HNA = 2:7:1, Etch time = 40 min, Rotation = 25 RPM.

5.1.2   Long slit experiments

Experiment C   The experiment environment of slit tests are similar as the dot test. In the Figure 5.5, the width at the top is higher than bottom within the channel and the wider part gathers at the top right of the wafer.

Figure 5.5: Plot of surface channel width distribution in a wafer. Plus signs indicate the width larger than median value of sample channels. HNA = 2:7:1, Etch time = 40 min, Rotation = 0 RPM.
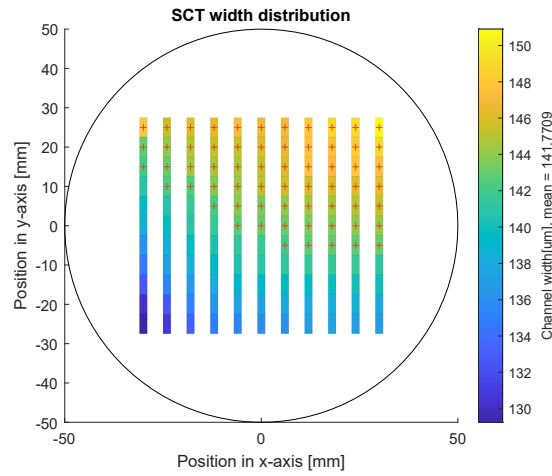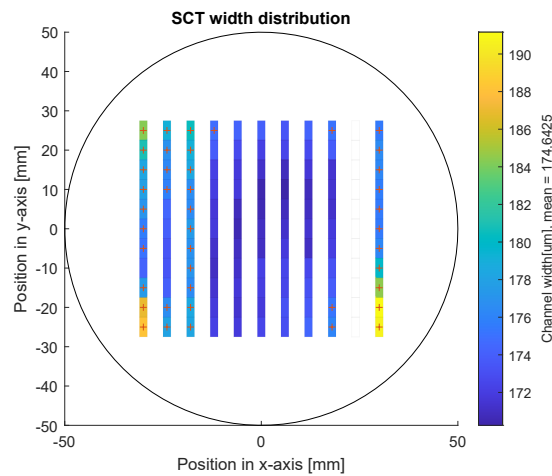
Experiment D   In Figure 5.6, the wider parts located close to the outer edge of the wafer, and the mean width is larger than the one without rotation. The 10th slot is omitted for the mean calculation because it has a larger difference from the rest slits. The top view of all slits looks like Figure 4.4b, but the 3rd and 10th slits, as shown in Figure 5.7a.

Figure 5.6: Plot of surface channel width distribution in a wafer. Plus signs indicate the width larger than median value of sample channels. HNA = 2:7:1, Etch time = 40 min, Rotation = 25 RPM.

The specific dimension of the slits is listed with 25 RPM in Table 5.1, based on the cross-section images. As can be seen from the third column, the values are equal to 1, which indicates that the semicircle's width is double of height.

The last column shows the area ratio between the semicircle profile and a circle calculated in terms of the half channel's width. If the value is equal to 0.5, then it demonstrates that the cross-section is a semicircle in terms of area. Therefore, the cross-section is considered a semicircle, when the W/2H is 1, the area ratio is 0.5, and it is a convex hull shape.

Table 5.1: Dimension of surface slits in the experiment D.

Channel	Width	Height	W/2H	Area ratio
1	185.93	93.67	0.992474	0.491
2	180.3	89.45	1.007826	0.500
3	181.71	91.26	0.995562	0.503
4	176.68	88.64	0.996616	0.501
5	175.28	89.25	0.981961	0.500
6	174.27	88.44	0.985244	0.505
7	173.87	89.05	0.976249	0.507
8	173.67	88.84	0.977431	0.502
9	174.67	90.05	0.96985	0.499
10	211.46	105.13	1.005707	0.506
11	176.28	89.05	0.989781	0.491

The 10th channel has a rough bottom(about $2.8\,\mu$m), as shown in Figure 5.7 so that the mid slit is black due to the diffuse of reflection in Figure 5.7a, instead of a shiny slit for a smooth bottom in other channels.

(a) (b)

(c) (d)
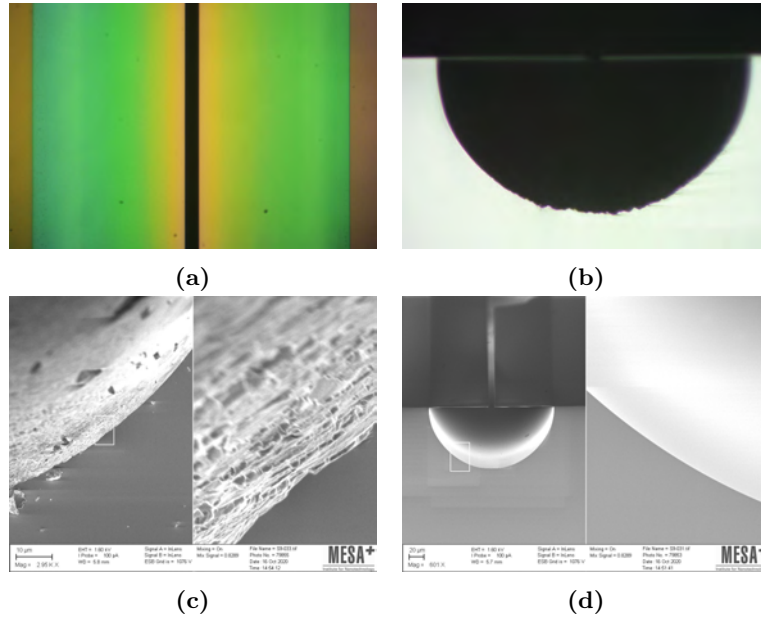
Figure 5.7: Optical microscope photographs of top view(a) and cross-sections(b) of 10th slit. SEM image of 10th channel's bottom(c) and smooth bottom of other channels(d)

5.1.3 Summary

According to the first four experiments, the results are listed in Table 5.2 and compare the experiments in terms of range, mean value, the normalized standard deviation in vertical and horizontal. At the last row, the etch rate is calculated in one direction.

Comparing dot experiments A and B, the agitation system positively affects the uniform etching result among the wafer, but the etch rate remains the same. Comparing slit experiments C and D, besides the unusual channels, the intervention of the rotation system helps to reduce the standard deviation of channel width much and increase the etch rate. As for the unusual 10th channel, it is wider and rougher than others. The local concentration of HNA changes and enters to a neighbor etched surface region with a higher HF concentration.

Table 5.2: Results of dots and slits experiments.

|	A	B	C	D[1]
Vertical Range (μm)	[90.50 97.79]	[91.46 95.88]		
Horizontal(width) Range (μm)	[91 98.09]	[91.91 96.23]	[129.25 150.9]	[170.25 191.16]
Vertical Mean (μm)	94.51	94.11		
Horizontal(width) Mean (μm)	94.65	94.21	141.77	174.64
SD/Vertical	1.39%	0.89%		
SD/Horizontal	1.42%	0.92%	3.14%	2.34%
Average etch rate (μm/min)	1.181	1.176	1.763	2.183

[1] The 10th channel is omitted.

5.2 Buried channel

The rest of the experiments are in regard to the buried channel. The biggest difference between the buried channel and surface channel is that the etchant has to pass through a trench with $10\,\mu$m width and $65\,\mu$m depth and etch the silicon. Therefore, this long trench may lead to different concentrations of HNA solution locally at the etching surface.

5.2.1 Experiments in 2:7:1 solution

Experiment E   In experiment E, the cross-section of the buried channel is concerned. Normally, the cross-sections look different depending on location in the wafer, classified by four types in Figure 5.8.

(a) O

(b) AO

(c) *

(d) *

(e) RO
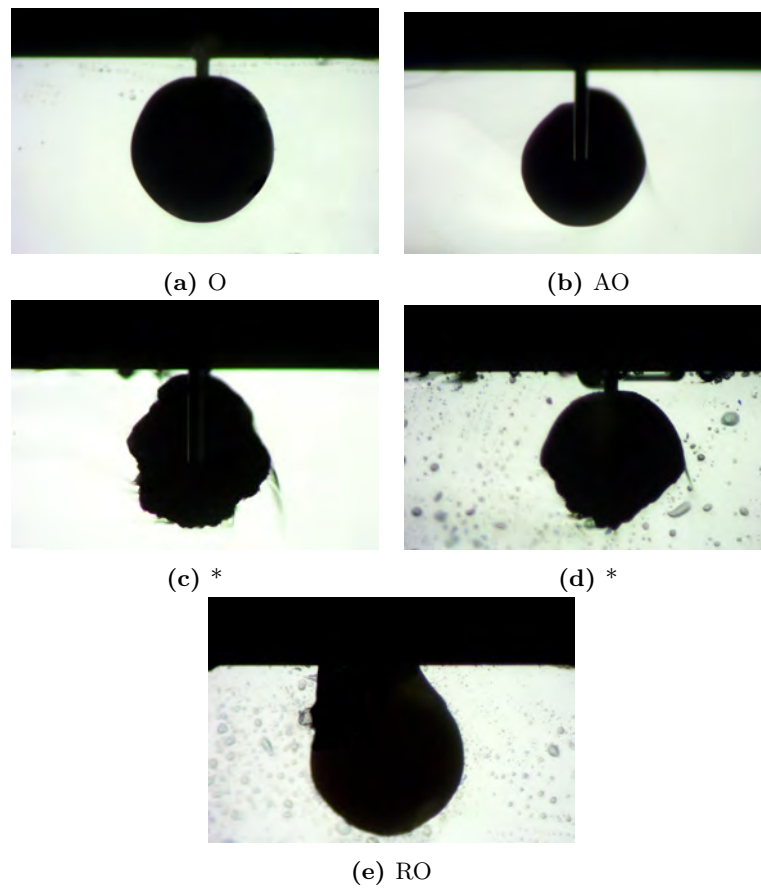
Figure 5.8: Optical microscope images of the cross-section of the buried channel in five different profiles. The sign in the caption of each sub-figure is the element in Figure 5.9.

In Figure 5.8, sub-figure (a) shows a symmetrical circular cross-section. (b) expresses an asymmetrical channel with a smooth surface on the rest. (c) indicates an incomplete cross-section with a rough surface. (d) demonstrates both rough and smooth surfaces in one cross-section, where the smooth is close to the upper part, and the rough imperfect locates at the bottom, also shown in Figure 5.10 from the cross-section along the channel. (e) can be seen as a circular cross-section and with some overetched from inner and the top of SiRN layer. The distribution of these five types among the wafer is shown in Figure 5.9.
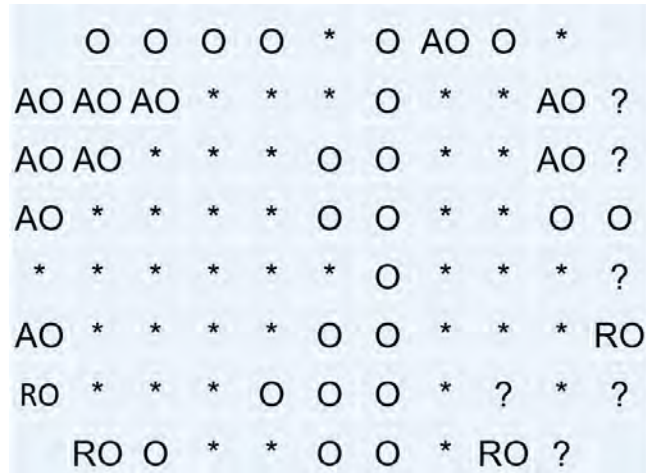
Figure 5.9: Distribution of buried channel etched by 2:7:1 for 90 min with 25 RPM among a wafer. The question marks indicate the unobservable. The columns indicate the eleven slits on a wafer and the row stands for the cross-section on each slits. The distance between two adjacent cut is 5-6 mm.
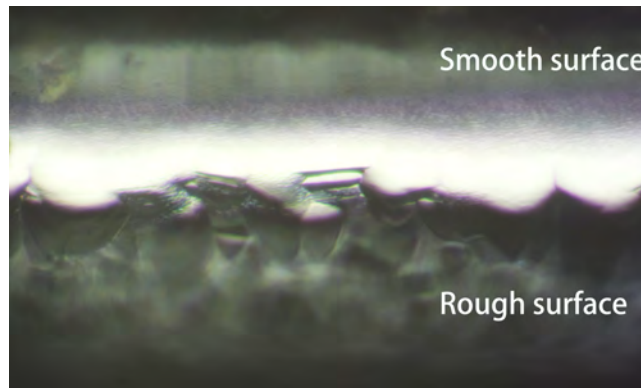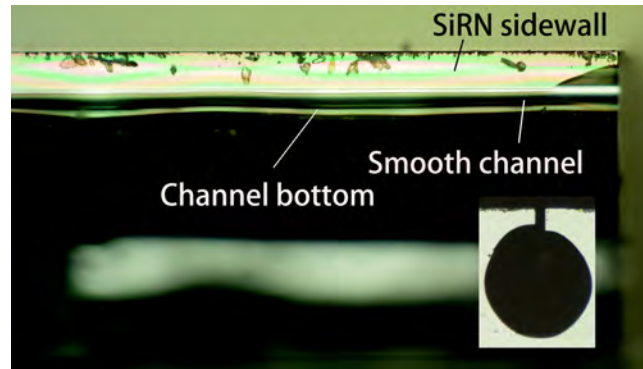

Figure 5.10: Optical microscope image of lengthwise-section along the channel for the boundary of the smooth upper and rough lower in one buried channel(Figure 5.8d).

The average height and width are around $100.2\,\mu$m and $100.3\,\mu$m, respectively, for the circular cross-section for 90 min so that the etch rate in one direction is $0.56\,\mu$m/min. The ratio of vertical and lateral etch rate is 1. The thickness SiRN layer on the sidewall is $0.8\,\mu$m. The obvious out of round is occupied 60% of all the observed channels.

However, the distribution among the wafer does not stand for the etching result of the whole wafer by these cross-sections because the number of samples is limited, and the sampling distance is large($6\,$mm in this case). Therefore, observing the roughness on the channel wall in the lengthwise-section along the channel might help to understand the etching result. On the basis of observing

experience, the smooth surface tends to give a nearly complete circular channel. Figure 5.11 illustrates the continuously smooth channel wall. In fact, the total distance of the continuous smooth channel is $3000\,\mu$m, at least.


Figure 5.11: Optical microscope images of lengthwise-section along the channel for the smooth channel and its corresponding cross-section.
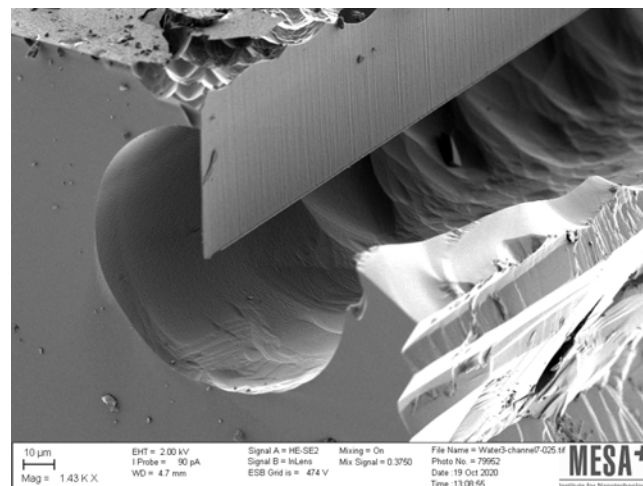
The inner wall of a channel is not always smooth. The transition of roughness is shown in Figure 5.12. The transition part is also observed by SEM(Figure 5.13).
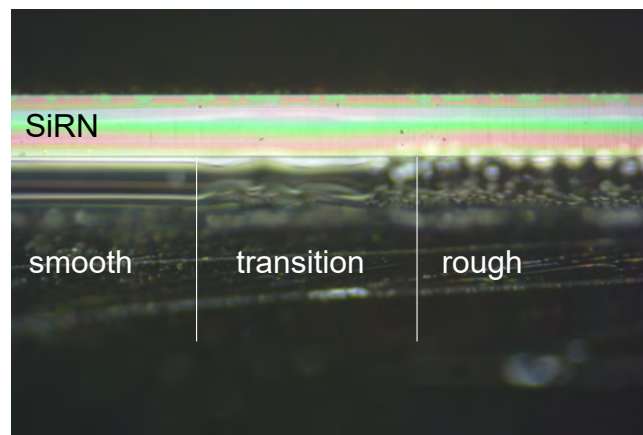
Figure 5.12: Optical microscope image of roughness transition along a channel.
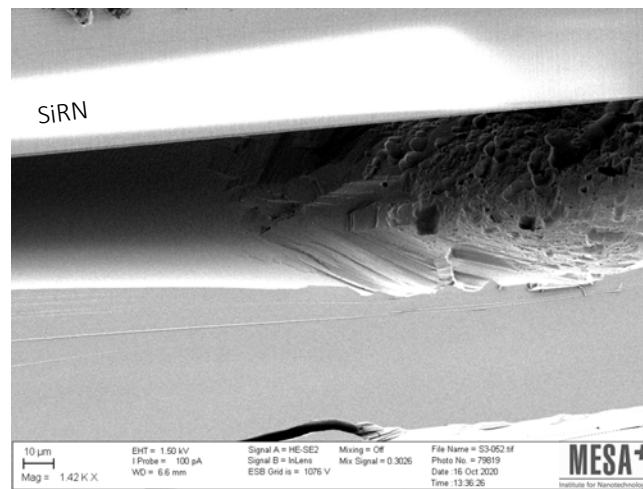
Figure 5.13: SEM image of roughness transition along a channel.

Figure 5.14: SEM image of buried channel in experiment E. An approximate roughness of the surface is $1.115\,\mu$m, as shown in Figure A.2.

Discussion

The experiment with 25 RPM in 2:7:1 compositions gives some circular buried channels with a smooth channel wall(Figures 5.8a, 5.8b and 5.8e) and some channels with incomplete cross-sections(Figures 5.8c and 5.8d).

For Figure 5.8b, there are two reasons why asymmetrical cross-section presents: 1. In the bottom removal process, the opening size might be different on both sides, especially the channel locating at the wafer's edge due to the directional RIE, resulting in the different starting etching surfaces. 2. The rotation tends to push the solution to one side.

Figure 5.8c shows a random shape of cross-section. At the low HF and high HNO_3 composition, the etch rate is controlled by the ability of HF to remove the SiO_2 when it is oxidized by HNO_3. Due to the rich HNO_3, the SiO_2 is easily formed on the surface of silicon. Therefore, the cause of random incomplete shape is the shortage of HF. As for Figure 5.8d, the upper channel is a semicircle, but the lower part is incomplete, which might show that the HF is consumed before it diffuses to the whole channel.

Figure 5.8e indicates that the SiRN layer on the top is etched too much by the plasma etching in the bottom removal process, as shown in Figure A.3. Consequently, the silicon is etched from both directions of the top and bottom.

The HNA solution in a 2:7:1 ratio tends to give a smooth surface. The rough surface is formed because the locate concentration varies into the adjacent surface topography zone of the HNA composition triangle, or the bubbles attached to the silicon surface prevent the isotropic etching.

5.2.2   Experiments in 3:6:1 solution

Experiment F   In experiment F, the HNA composition changes from 2:7:1 to 3:6:1 because the experiment with 2:7:1 showed some incomplete cross-sections. The rotation rate is reduced to 10 RPM. According to the observation results, the apparent out-of-round occupied 32% of all cross-sections, which is much less than 2:7:1, and its distribution is shown in Figure 5.16. The majority of round cross-sections gather at the center of the wafer. However, compared with the 2:7:1 composition, all of the cross-sections have the obvious roughness at the bottom.

(a)

(b)

(c)

(d)

(e)
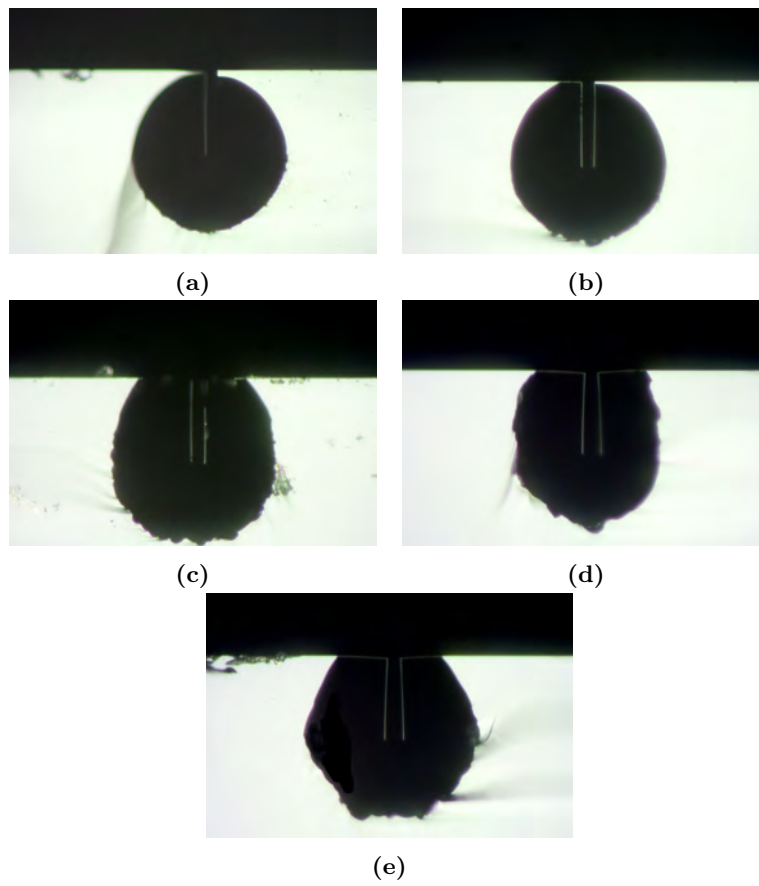
Figure 5.15: Optical microscope image of buried channel etched in 3:6:1 composition in Coriolis shape pattern.

	C1	C2	C3	C4	C5	C6	C7	C8	C9	10	11
R1											
R2		O			O		O	O	O		
R3				O	O	O	O	O	O		
R4	O		O		O	O	O	O	O	O	O
R5	O	O	O	O	O	O		O		O	
R6	O		O	O	O	O		O	O	O	
R7		O	O	O		O	O	O	O	O	
R8			O	O							

Figure 5.16: Distribution of buried channel etched by 3:6:1 for 90 min with 10 RPM among a wafer. Os stand for round cross-sections, which also include the overetched based on a round shape.

The average width of cross-section is $113.7\,\mu$m and the lateral etching rate is $0.631\,\mu$m/min. The average height of cross-section is $116.4\,\mu$m and the vertical etching rate is $0.647\,\mu$m/min. However, the statistic results on vertical are not accurate because most of the channels are overetched to the protection layer. Even so, the vertical etching rate is higher than the lateral. The thickness SiRN layer on the sidewall is $0.7\,\mu$m remained.
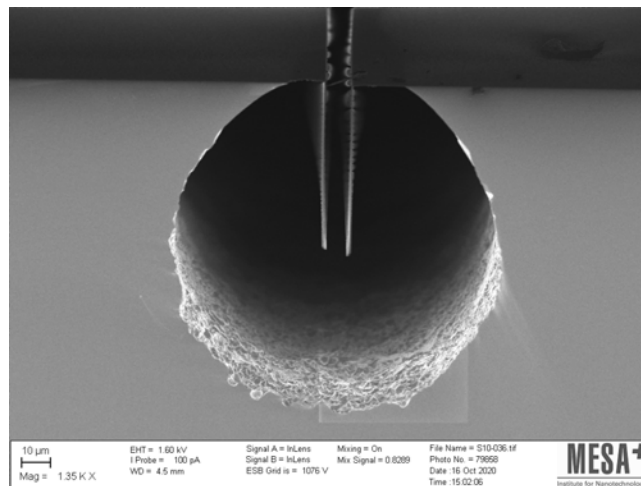
Figure 5.17: SEM image of buried channel in 3:6:1.

Discussion

Comparing with the 2:7:1 experiment, the 3:6:1 composition has a higher concentration of HF, which etches more complete channels. That would explain that sometimes the HF is not sufficient in the buried channel locally with 2:7:1

solution. However, the rough surface in the complete channel is apparent, especially at the bottom, and some of the cross-sections show the smooth upper and rough lower profiles.

5.2.3   Summary

Table 5.3: Comparison between experiments E and F in terms of compositions, etch rate, SiRN etched, and the percentage of out of round over all cross-sections in the wafer.

ID	Composition	etch rate μm/min	SiRN layer etched[μm]	Out of Round
E	2:7:1	0.56	0.2	60%
F	3:6:1	0.64	0.3	32%

Based on the experiment results, 3:6:1 composition has a higher etch rate and less incomplete round cross-sections than 2:7:1, but 2:7:1 has a more specular surface. Usually, the rough channel walls could give a relatively high hydraulic resistance to the microfluidic, compared with smooth channel walls, and some of the particles inevitably hit against the rough surface. Therefore, the smooth channel wall is preferred for microfluidic measurement. In this concentration of smooth etched surface region, increasing the HF concentration between 2:7:1 and 3:6:1 could help to increase the etch rate to reduce the cumulative error in a long reaction time and etch more complete round cross-sections with a smooth surface. The experiments done could not draw the full conclusion, and more experiments should be done to investigate the relation between etching parameters and the etching result for the buried channels.

Chapter 6

Conclusion and future works

6.1   Conclusion

A round channel of the micro Coriolis massflow sensor is preferred because the channel will deform with pressure isotropically, and the flow rate is measured in an ideal way. A round channel can be formed by dry etching or wet etching based on the buried channel technology. Dry etching for the buried channel is not efficient in large diameter and costs a lot. HNA solution, as the wet isotropic etchant, could etch the round channel with a smooth surface underneath the wafer on a low-budget. An etching bath with a rotation system is designed, built, and used in the wet etching process to increase the uniformity of devices on the wafer level. A manual is written down for guiding the operators to use the etching bath properly. Experiments with two HNA compositions is to characterize the HNA solution for a buried structure under a trench with $10\,\mu$m width and $65\,\mu$m depth. A $100\,\mu$m diameter channel with a specular surface can be formed.

6.2   Future works

Further verification can be split into two ways:

1. Try the HNA solution in different compositions. Based on 2:7:1, the HF concentration can be increased slightly but not larger than 3:6:1, 2.5:6.5:1, for instance. That could have advantages of both compositions – more complete channels with a smooth surface. Alternatively, increasing the temperature can increase the diffusion rate of etchant and species exchange via the trench with a high aspect ratio.

2. According to experiments C and D, two surface semicircle channels can be bonded together to form a nearly perfect round channel with a larger diameter.
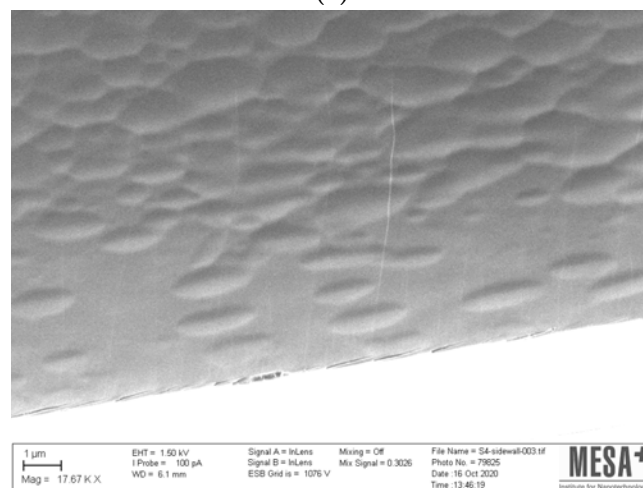
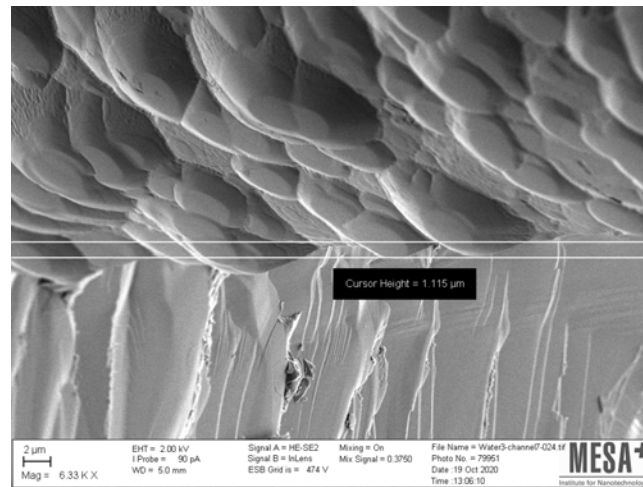# Appendices

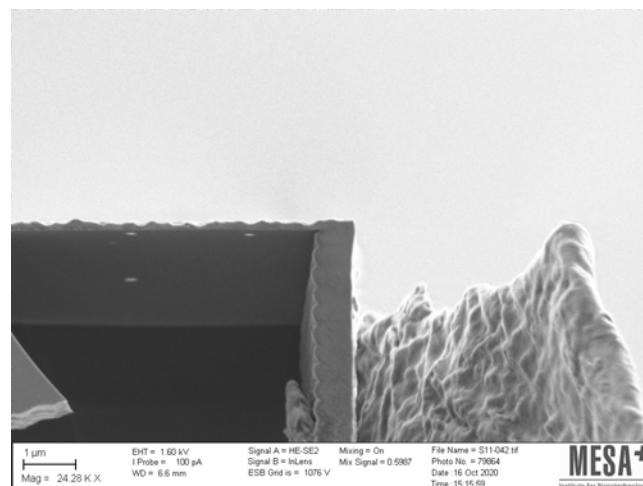# Appendix A

Supplementary SEM image
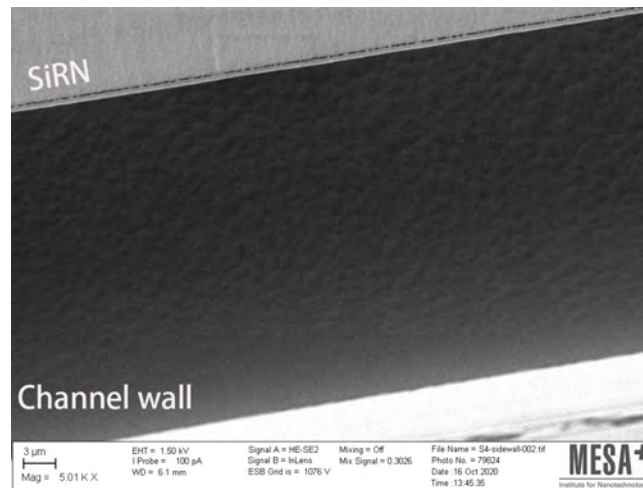
(a)

(b)

Figure A.1: SEM images of the smooth surface on the channel wall in experiment E.

Figure A.2: SEM image of the channel surface in experiment E. An approximate roughness of the surface is $1.115\,\mu$m
.

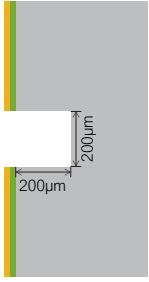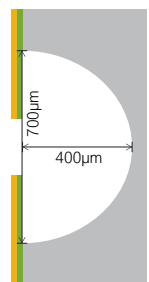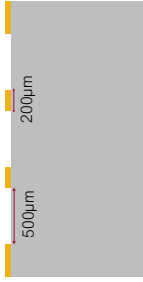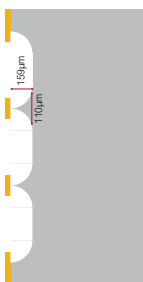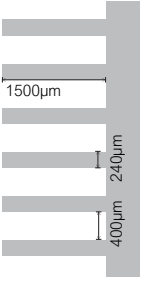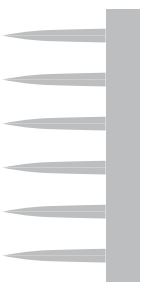**Figure A.3:** SEM image of the holes on the SiRN layer
.

Appendix B

Parameters of the applications in literature review

Table B.1: Summary of the preparation before wet isotropic etching process of each mentioned application.

Articles	Applications	Mask material	Wafer orientation	Before wet etching	After wet etching
Bai et al. [32]	Toroidal mold	Si_3N_4	Upwards		
Kim [33]	Wafer thinning	maskless	Upwards	-	-
Hamzah et al. [49]	Microneedles	Si_3N_4	Against the tangent		
Bauhuber et al. [44]	Deep channels	Si_3N_4	Upwards	not mention	not mention
Bhandari et al. [50]	Utah electrodes array	maskless	Downwards		

* Green indicates SiO_2.
** Yellow indicates Si_3N_4.

Table B.2: Summary of the etching parameters and evaluations of each mentioned application.

Articles	HNA composition	Temperature °C	Agitation (RPM)	Magnetic stir (RPM)	Mask selectivity	Etching rate (μm/min)	Uniformity	Roughness
Bai et al. [32]	2.5:7:1	30	20	-	520:1	3.5	99.87%	<10 nm
Kim [33]	3:5:3	-	15	-	-	8	96%	-
	35:45:20	-	15	-	-	11	96%	-
	1:4:3	-	60	-	-	2.5	98%	-
Hamzah et al. [49]	2:7:1	30	-	350	-	15	-	-
Bauhuber et al. [44]	2:7:1	25.5	-	60	-	0	98.33%	-10 nm
Bhandari et al. [50]	1:19	0	22	500	> 1000 : 1	25	98.7%	-

*dummy .
** dummy.

78

Bibliography

[1] J. T. W. Kuo, L. Yu, and E. Meng, "Micromachined thermal flow sensors—a review," *Micromachines*, vol. 3, no. 3, pp. 550–573, jul 2012.

[2] Y.-H. Wang, C.-P. Chen, C.-M. Chang, C.-P. Lin, C.-H. Lin, L.-M. Fu, and C.-Y. Lee, "MEMS-based gas flow sensors," *Microfluidics and Nanofluidics*, vol. 6, no. 3, pp. 333–346, jan 2009.

[3] R. Wiegerink, T. Lammerink, M. Dijkstra, and J. Haneveld, "Thermal and coriolis type micro flow sensors based on surface channel technology," *Procedia Chemistry*, vol. 1, no. 1, pp. 1455–1458, sep 2009.

[4] J. Groenesteijn, "Microfluidic platform for coriolis-based sensor and actuator systems," Ph.D. dissertation, 2016.

[5] P. Enoksson, "Novel resonant micromachined silicon devices for fluid applications," *Instrumentation Laboratory, Department of Signals, Sensors and Systems Royal Institute of Technology, Sweden*, 1997.

[6] P. Enoksson, G. Stemme, and E. Stemme, "A silicon resonant sensor structure for coriolis mass-flow measurements," *Journal of Microelectromechanical Systems*, vol. 6, no. 2, pp. 119–125, jun 1997.

[7] Y. Zhang, S. Tadigadapa, and N. Najafi, "A micormachined coriolis-force-based mass flowmeter for direct mass flow and fluid density measurement," in *Transducers '01 Eurosensors XV*. Springer Berlin Heidelberg, 2001, pp. 1432–1435.

[8] D. Sparks, R. Smith, M. Straayer, J. Cripe, R. Schneider, A. Chimbayo, S. Anasari, and N. Najafi, "Measurement of density and chemical concentration using a microfluidic chip," *Lab on a Chip*, vol. 3, no. 1, p. 19, 2003.

[9] R. Smith, D. Sparks, D. Riley, and N. Najafi, "A MEMS-based coriolis mass flow sensor for industrial applications," *IEEE Transactions on Industrial Electronics*, vol. 56, no. 4, pp. 1066–1071, apr 2009.

[10] J. Haneveld, T. Lammerink, M. Dijkstra, H. Droogendijk, M. de Boer, and R. Wiegerink, "Highly sensitive micro coriolis mass flow sensor," in *2008 IEEE 21st International Conference on Micro Electro Mechanical Systems*. IEEE, jan 2008.

[11] J. Haneveld, T. Lammerink, M. de Boer, and R. Wiegerink, "Micro coriolis mass flow sensor with integrated capacitive readout," in *2009 IEEE 22nd*

International Conference on Micro Electro Mechanical Systems. IEEE, jan 2009.

[12] J. Haneveld, T. S. J. Lammerink, M. J. de Boer, R. G. P. Sanders, A. Mehendale, J. C. Lötters, M. Dijkstra, and R. J. Wiegerink, "Modeling, design, fabrication and characterization of a micro coriolis mass flow sensor," *Journal of Micromechanics and Microengineering*, vol. 20, no. 12, p. 125001, nov 2010.

[13] M. Dijkstra, M. J. de Boer, J. W. Berenschot, T. S. J. Lammerink, R. J. Wiegerink, and M. Elwenspoek, "A versatile surface channel concept for microfluidic applications," *Journal of Micromechanics and Microengineering*, vol. 17, no. 10, pp. 1971–1977, sep 2007.

[14] R. Monge, J. Groenesteijn, D. Alveringh, R. Wiegerink, J. Lötters, and L. J. Fernandez, "Su-8 micro coriolis mass flow sensor," *Sensors and Actuators B: Chemical*, vol. 241, pp. 744–749, mar 2017.

[15] M. de Boer, R. Tjerkstra, J. Berenschot, H. Jansen, G. Burger, J. Gardeniers, M. Elwenspoek, and A. van den Berg, "Micromachining of buried micro channels in silicon," *Journal of Microelectromechanical Systems*, vol. 9, no. 1, pp. 94–103, mar 2000.

[16] M. Dijkstra, M. de Boer, J. Berenschot, T. Lammerink, R. Wiegerink, and M. Elwenspoek, "Miniaturized thermal flow sensor with planar-integrated sensor structures on semicircular surface channels," *Sensors and Actuators A: Physical*, vol. 143, no. 1, pp. 1–6, may 2008.

[17] D. Alveringh, T. V. P. Schut, R. J. Wiegerink, W. Sparreboom, and J. C. Lotters, "Resistive pressure sensors integrated with a coriolis mass flow sensor," in *2017 19th International Conference on Solid-State Sensors, Actuators and Microsystems (TRANSDUCERS)*. IEEE, jun 2017.

[18] D. Alveringh, R. J. Wiegerink, and J. C. Lotters, "Integrated pressure sensing using capacitive coriolis mass flow sensors," *Journal of Microelectromechanical Systems*, vol. 26, no. 3, pp. 653–661, jun 2017.

[19] J. Groenesteijn, M. J. de Boer, J. C. Lötters, and R. J. Wiegerink, "A versatile technology platform for microfluidic handling systems, part II: channel design and technology," *Microfluidics and Nanofluidics*, vol. 21, no. 7, jul 2017.

[20] X.-Q. Wang, X. Yang, K. Walsh, and Y.-C. Tai, "Gas-phase silicon etching with bromine trifluoride," in *Proceedings of International Solid State Sensors and Actuators Conference (Transducers '97)*. IEEE, 1997.

[21] U. Koehler, A. E. Guber, W. Bier, M. Heckele, and T. Schaller, "Fabrication of microlenses by combining silicon technology, mechanical micromachining and plastic molding," in *Miniaturized Systems with Micro-Optics and Micromechanics*, M. E. Motamedi, Ed. SPIE, mar 1996.

[22] G. Kovacs, N. Maluf, and K. Petersen, "Bulk micromachining of silicon," *Proceedings of the IEEE*, vol. 86, no. 8, pp. 1536–1551, 1998.

[23] P. Chu, J. Chen, R. Yeh, G. Lin, J. Huang, B. Warneke, and S. Pister, "Controlled pulse-etching with xenon difluoride," in *Proceedings of International Solid State Sensors and Actuators Conference (Transducers '97)*. IEEE, 1997.

[24] K. Sugano and O. Tabata, "Effects of aperture size and pressure on XeF$_2$ etching of silicon," *Microsystem Technologies*, vol. 9, no. 1-2, pp. 11–16, nov 2002.

[25] ——, "Reduction of surface roughness and aperture size effect for etching of si with XeF$_2$," *Journal of Micromechanics and Microengineering*, vol. 12, no. 6, pp. 911–916, oct 2002.

[26] C. Easter and C. O'Neal, "Characterization of high-pressure XeF$_2$ vapor-phase silicon etching for MEMS processing," *Journal of Microelectromechanical Systems*, vol. 18, no. 5, pp. 1054–1061, oct 2009.

[27] D. Xu, B. Xiong, G. Wu, Y. Wang, X. Sun, and Y. Wang, "Isotropic silicon etching with XeF$_2$ gas for wafer-level micromachining applications," *Journal of Microelectromechanical Systems*, vol. 21, no. 6, pp. 1436–1444, dec 2012.

[28] Y. Saito, "Characteristics of plasmaless dry etching of silicon-related materials using chlorine trifluoride gas," *Sens. Mater*, vol. 14, no. 5, 2002.

[29] J. Groenesteijn, M. de Boer, J. van Putten, W. Sparreboom, J. Lotters, and R. Wiegerink, "Fabrication of free-hanging tubes for a high flow micro coriolis mass flow meter," *MNE conference*, Sep. 2019.

[30] Y. H. Lee and M. R. Polcari, *Properties of Silicon (Emis Datareviews Series, No 4), Chapter 23*. Inst of Engineering & Technology, 1988.

[31] W. C. Hui, "How to prevent a runaway chemical reaction in the isotropic etching of silicon with HF/HNO$_3$/CH$_3$COOH or HNA solution," in *Device and Process Technologies for MEMS, Microelectronics, and Photonics III*, J.-C. Chiao, A. J. Hariz, D. N. Jamieson, G. Parish, and V. K. Varadan, Eds. SPIE, apr 2004.

[32] Z. Bai, Y. Wang, Q. Zhao, Z. Yang, J. Cui, and G. Yan, "Improved HNA isotropic etching for large-scale highly symmetric toroidal silicon molds with <10-nm roughness," *Journal of Micro/Nanolithography, MEMS, and MOEMS*, vol. 18, no. 04, p. 1, oct 2019.

[33] Y. Kim, "Experimental study on etching characteristics of a spin-etching method," *Journal of Microelectromechanical Systems*, vol. 24, no. 6, pp. 1827–1831, dec 2015.

[34] B. Schwartz, "Chemical etching of silicon: IV. etching technology," *Journal of The Electrochemical Society*, vol. 123, no. 12, p. 1903, 1976.

[35] M. J. Madou, *Manufacturing Techniques for Microfabrication and Nanotechnology*. Taylor & Francis Inc, 2011.

[36] P. Pal, *Silicon wet bulk micromachining for MEMS*. Singapore: Pan Stanford Publishing, 2017.

[37] T. Doi, *Advances in CMP/polishing technologies for the manufacture of electronic devices.* Oxford: William Andrew, 2012.

[38] H. Robbins and B. Schwartz, "Chemical etching of silicon: I . the system HNO_3, HF, and H_2O," *Journal of The Electrochemical Society*, vol. 106, no. 6, p. 505, 1959. [Online]. Available: https://doi.org/10.1149%2F1.2427397

[39] ——, "Chemical etching of silicon: II . the system HNO_3, HF, H_2O and $HC_2H_3O_2$," *Journal of The Electrochemical Society*, vol. 107, no. 2, p. 108, 1960. [Online]. Available: https://doi.org/10.1149%2F1.2427617

[40] B. Schwartz and H. Robbins, "Chemical etching of silicon: III . a temperature study in the acid system," *Journal of the electrochemical society*, vol. 108, no. 4, p. 365, 1961.

[41] M. Steinert, J. Acker, M. Krause, S. Oswald, and K. Wetzig, "Reactive species generated during wet chemical etching of silicon in HF/HNO3mixtures," *The Journal of Physical Chemistry B*, vol. 110, no. 23, pp. 11 377–11 382, jun 2006.

[42] G. Kovacs, *Micromachined transducers sourcebook.* Boston: WCB/McGraw-Hill, 1998.

[43] K. Petersen, "Silicon as a mechanical material," *Proceedings of the IEEE*, vol. 70, no. 5, pp. 420–457, may 1982.

[44] M. Bauhuber, A. Mikrievskij, and A. Lechner, "Isotropic wet chemical etching of deep channels with optical surface quality in silicon with HNA based etching solutions," *Materials Science in Semiconductor Processing*, vol. 16, no. 6, pp. 1428–1433, dec 2013.

[45] M. W. Jenkins, "A new preferential etch for defects in silicon crystals," *Journal of The Electrochemical Society*, vol. 124, no. 5, p. 757, 1977.

[46] Y. Liu, W. Zhang, J. Tang, Y. Wang, Y. Xing, and D. Sun, "The silicon nitride mask for isotropic wet etching," *Semiconductor Optoelectronics*, vol. 37, pp. 495–498, 08 2016.

[47] J. Albero, L. Nieradko, C. Gorecki, H. Ottevaere, V. Gomez, H. Thienpont, J. Pietarinen, B. Päivänranta, and N. Passilly, "Fabrication of spherical microlenses by a combination of isotropic wet etching of silicon and molding techniques," *Optics Express*, vol. 17, no. 8, p. 6283, apr 2009.

[48] H. Hashimoto, S. Tanaka, and K. Sato, "Silicon acoustic lens for scanning acoustic microscope (SAM)," in *TRANSDUCERS '91: 1991 International Conference on Solid-State Sensors and Actuators. Digest of Technical Papers.* IEEE, 1991.

[49] A. A. Hamzah, N. A. Aziz, B. Y. Majlis, J. Yunas, C. F. Dee, and B. Bais, "Optimization of HNA etching parameters to produce high aspect ratio solid silicon microneedles," *Journal of Micromechanics and Microengineering*, vol. 22, no. 9, p. 095017, aug 2012.

[50] R. Bhandari, S. Negi, L. Rieth, and F. Solzbacher, "A wafer-scale etching technique for high aspect ratio implantable MEMS structures," *Sensors and Actuators A: Physical*, vol. 162, no. 1, pp. 130–136, jul 2010.

[51] L. C. Fegely, D. N. Hutchison, and S. A. Bhave, "Isotropic etching of 111 SCS for wafer-scale manufacturing of perfectly hemispherical silicon molds," in *2011 16th International Solid-State Sensors, Actuators and Microsystems Conference.* IEEE, jun 2011.

[52] Polyfluor, "generial properties of fluoropolymer." [Online]. Available: https://www.polyfluor.nl/en/materials/ (Date last accessed 09-Sep-2014).

[53] H. Soemers, *Design principles : for precision mechanisms.* S.l: Herman Soemers, 2011.